



## Prediction capability of Pareto optimal solutions: A multi-criteria optimization strategy based on model capability ratios



Lucas Guedes de Oliveira<sup>\*</sup>, Anderson Paulo de Paiva, Paulo Henrique da Silva Campos, Emerson José de Paiva, Pedro Paulo Balestrassi

*Institute of Industrial Engineering and Management, Federal University of Itajuba, Itajuba, Minas Gerais, Brazil*

### ARTICLE INFO

#### Keywords:

Prediction variance  
Model capability ratios  
Design of experiments  
Response surface methodology  
Normal boundary intersection  
Multiobjective optimization

### ABSTRACT

Response Surface Methodology is an effective framework for performing modelling and optimization of industrial processes. The Central Composite Design is the most popular experimental design for response surface analyses given its good statistical properties, such as decreasing prediction variance in the design center, where it is expected to find the stationary points of the regression models. However, the common practice of reducing center points in response surface studies may damage this property. Moreover, stationary and optimum points are rarely the same in manufacturing processes, for several reasons, such as saddle-shaped models, convexity incompatible with optimization direction, conflicting responses, and distinct convexities. This means that even when the number of center points is appropriate, the optimal solutions will lie in regions with larger prediction variance. Considering that, in this paper, we advocate that the prediction variance should also be considered into multiobjective optimization problems. To do this, we propose a multi-criteria optimization strategy based on capability ratios, wherein (1) the prediction variance is taken as the natural variability of the model and (2) the differences of expected values to nadir solutions are taken as the allowed variability. Normal Boundary Intersection method is formulated for performing the optimization of capability ratios and obtaining the Pareto frontiers. To illustrate the feasibility of the proposed approach, we present a case study of the turning without cutting fluids of AISI H13 steel with wiper CC650 tool. The results have supported that the proposed approach was able to find a set of optimal solutions with satisfactory prediction capabilities for both responses of interest (tool life  $T$  and surface roughness  $Ra$ ), for a case with reduced number of center points, a saddle-shaped function for  $T$  and a convex function for  $Ra$ , with conflicting objectives. Although it was a response more difficult to control, the optimization benefited more  $Ra$ , which was a desired result. Finally, we also provide the sample sizes to detect differences between Pareto optimal solutions, allowing the decision maker to find distinguishable solutions at given levels of risk.

### 1. Introduction

Response Surface Methodology (RSM) is a framework widely used in the modelling and optimization of industrial processes [1–3]. In essence, RSM employs statistical and mathematical techniques and methods to estimate response variables as a function of explanatory factors by using planned experiments [4]. Often, second-order models are employed to estimate a given region of interest of a response with some explanatory factors. The core idea is that these models are used as objective functions in optimization problems, providing the real values of the factors that effectively improve the processes.

The Central Composite Design (CCD) is recognized in the literature

as the most popular second-order design for RSM experimental studies because of its good statistical properties [5]. The CCD combines three types of points to allow the estimation of the main effects and their interactions (factorial points), the quadratic effects (axial points) and the error component (center points). Additionally, the CCD offers the minimum prediction variance in the design center [6], since the stationary is expected to be the optimal point and lie in the central region of the design. Nevertheless, these assumptions are not always true in real cases.

First, when using the CCD, the number of center points recommended [7] is often reduced [8–10] which leads to profound modifications in the prediction variance functions, thus impacting on

<sup>\*</sup> Corresponding author.

*E-mail addresses:* [lucasguedesdeoliveira@gmail.com](mailto:lucasguedesdeoliveira@gmail.com) (L.G. de Oliveira), [andersonppaiva@unifei.edu.br](mailto:andersonppaiva@unifei.edu.br) (A.P. de Paiva), [paulohcampos@unifei.edu.br](mailto:paulohcampos@unifei.edu.br) (P.H. da Silva Campos), [emersonpaiva@unifei.edu.br](mailto:emersonpaiva@unifei.edu.br) (E.J. de Paiva), [ppbalestrassi@gmail.com](mailto:ppbalestrassi@gmail.com) (P.P. Balestrassi).

<https://doi.org/10.1016/j.precisioneng.2019.06.008>

Received 27 March 2019; Received in revised form 25 May 2019; Accepted 19 June 2019

Available online 27 July 2019

0141-6359/ © 2019 Elsevier Inc. All rights reserved.

the ability of the response surface models to represent the real processes [11].

Second, many response surface models of manufacturing processes are saddle-shaped [12–14] or have optimization directions incompatible with convexities (maximize convex functions: [15,16]; or minimize concave functions [1,17]); this implies that for these cases the stationary point will not be the optimum, which will be taken to regions farther away from the design center, where the prediction variance is naturally greater.

Finally, it is common to find problems in which multiple response variables with conflicting objectives need to be optimized [18–20]. In these cases, the optimal solution will tend to regions of greater variance, at least for one of the responses.

Considering the distortions caused in the prediction variance by the reduction of center points, by the incompatibility between the convexity and the optimization direction or by the optimization of multiple responses are usually disregarded in process studies, researchers may incur the error of optimizing a process in regions with high prediction variance, reducing, in this way, the probability of reproducing in practice the results obtained in the optimization.

In this sense, we consider that the optimization problems should also take into account the prediction variance of the models so that Pareto optimal solutions provide good prediction capabilities for all the investigated responses. Since the position of the point in the design space is subject to a given amount of variance [21], we argue that capable solutions can be obtained by shifting the optimal point, so that the variance is reduced without greatly changing the desired mean value of each response variable.

For this, in this work, we propose an optimization strategy based on modified capability ratios, in which the variances of the models are taken as the components of natural variability, while the differences between the expected values and the nadir points are taken as the components of allowed variability. Given its advantages in obtaining evenly distributed Pareto frontier, for the optimization of the capability ratios, we employ the Normal Boundary Intersection (NBI) method combined with the Gradient Reduced Generalized (GRG) algorithm. Also, we develop the sample sizes for detecting differences between Pareto optimal solutions according to the risk probability that the decision maker is willing to assume.

To report our research work, this paper is organized as follows: Section 2 focuses on design of experiments and prediction variance. Section 3 describes the process capability analysis. Section 4 describes the multiobjective optimization and the NBI method. Section 5 introduces the proposed multi-criteria optimization strategy based on capability ratios. Section 6 presents a case study for the optimization of turning of AISI H13 hardened steel with ceramic wiper insert. In Section 7 the main conclusions and the research opportunities for future works are drawn.

## 2. Design of experiments and prediction variance

The Design of Experiments (DOE) consists of the application of mathematical and statistical concepts for the generation of efficient experimental designs. The idea of design efficiency is that robust analyses can be performed based on a few experiments as possible. According to Myers and Montgomery [22], among the most common DOE techniques are factorial designs, mixture designs, Taguchi arrays, and response surface methodology (RSM).

The RSM is widely used for process optimization because it provides a sequence of oriented steps that cover the planning of the experiments, the modelling of functions using empirical data and the application of optimization methods [4,23]. The first step in the application of RSM is

to identify the parameters influencing the process and their respective levels. Then, it is necessary to define the experimental design to be used and perform the data collection. With the application of statistical techniques, it is possible to analyze the influence of the parameters on the responses of interest and to identify the most relevant process factors.

The central composite design (CCD) is recognized as the most widely used response surface design in experimental studies, given the advantages of modelling when using factorial, axial and center points [22]. A response surface model relating a given response variable of interest to its control parameters is usually expressed by a Taylor polynomial truncated in second-order terms, as shown in Eq. (1):

$$Y(\mathbf{x}) = \hat{Y}(\mathbf{x}) + \varepsilon = \beta_0 + \sum_{i=1}^k \beta_i x_i + \sum_{i=1}^k \beta_{ii} x_i^2 + \sum_{i < j} \beta_{ij} x_i x_j + \varepsilon \quad (1)$$

where:  $Y(\mathbf{x})$  is the function of interest,  $\hat{Y}(\mathbf{x})$  is the empirical model estimated from experimental data,  $\beta_0$  the constant term of the model,  $\beta_i$  are the coefficients of the linear terms,  $\beta_{ii}$  are the coefficients of the quadratic terms,  $\beta_{ij}$  are the coefficients of the interaction terms and  $\varepsilon$  is the residual, also known as the random error of the model, expected to be normally distributed with mean  $\mu = E(\varepsilon) = 0$  and known variance  $Var(\varepsilon) = \sigma^2$ , such that:  $\varepsilon \sim N(0, \sigma^2)$ .

The accuracy of Eq. (1) is essentially determined by two components: (1) the observational variance, which is influenced by the stochastic nature of the phenomena studied and the measurement system used for data collection, and (2) the design variance, which is influenced by the structure of the experimental design; in CCD, the number of factors, the number of each type of point (factorial, axial and center), and the radius of the design are the most relevant aspects. For the investigation of second-order rotatable designs, Box and Hunter [7] defined the general design variance function considering the CCD is designed in terms of  $(-1)$  and  $(+1)$  levels:

$$Var[\hat{Y}(\rho)] = \frac{2(k+2)\lambda_4^2 + 2\lambda_4(\lambda_4 - 1)(k+2)\rho^2 + [(k+1)\lambda_4 - (k-1)]\rho^4}{2\lambda_4[(k+2)\lambda_4 - k]} \quad (2)$$

Where  $\rho = \sqrt[4]{2^k}$  is the radius of rotatable CCD with  $k$  factors, and  $\lambda_4$  is the mixed fourth-order moment.

Box and Hunter [7] verified that the most significant aspect in response surface designs is that the variance function is as “low” and “flat” as possible everywhere in the experimental region. Considering that  $k$  depends on the phenomena investigated and the number of factorial and axial points are set, respectively,  $n_f = 2^k$  and  $n_s = 2k$ , the researchers proposed the values of  $\lambda_4$  that guarantee the “Uniform Precision” (UP) for different values of  $k$ :

$$\lambda_4 = \frac{(k+3) + \sqrt{9k^2 + 14k - 7}}{4(k+2)} \quad (3)$$

Based on this property, the appropriate numbers of center points are derived as follows:

$$n_0 = \{[2^k + 4(2^{k/2}) + 4]\lambda_4\} - (2^k + 2k) \quad (4)$$

Considering Eqs. (2)–(4), any reduction in the number of design points or modification in the radius of the design implies that the variance will be larger at least in some regions of the design and, therefore, the accuracy of the model will be reduced. Table 1 provides the recommended values of design points and design radius according to Box and Hunter [7].

To obtain the coefficients  $\beta$  of the model shown in Eq. (1), it is common to use the Ordinary Least Squares (OLS) method. The OLS

**Table 1**  
Recommended values of design points and design radius.  
Source: Adapted from Box and Hunter [7].

k	2	3	4	5
$\lambda_4$	0.7844	0.8385	0.8705	0.8918
$n_0$ (UP)	4.55	5.55	7.34	10.28
$n_0$ (UP) <sup>a</sup>	5	6	7	10
Factorials	4	8	16	32
Axials	4	6	8	10
N (UP)	13	20	31	52
$\rho$	1.41	1.68	2.00	2.38

<sup>a</sup> Values recommended by Ref. [7] after rounding.

estimator is obtained by minimizing the sum of squares of the residuals (which are, in practice, the differences between the measured values  $Y(\mathbf{x})$  and the estimated values  $\hat{Y}(\mathbf{x})$  in the experimental runs), such that:

$$\min_{\beta} L = \sum_{r=1}^n \varepsilon_r^2 = \sum_{r=1}^n (Y_r - \beta_0 + \sum_{i=1}^k \beta_i x_{ir} + \sum_{i=1}^k \beta_{ii} x_{ir}^2 + \sum_{i<j} \sum \beta_{ij} (x_i x_j)_r)^2 \quad (5)$$

where  $r$  designates the experimental run (or design row). For each run, there will be a residual  $\varepsilon_r$ .

In matrix notation:

$$\min_{\beta} L = \mathbf{Y}^T \mathbf{Y} - \beta^T \mathbf{X}^T \mathbf{Y} - \mathbf{Y}^T \mathbf{X} \beta + \beta^T \mathbf{X}^T \mathbf{X} \beta \quad (6)$$

where:

$$\tilde{\Sigma}_{\hat{\beta}} = \begin{matrix} & (\beta_0) & (\beta_1) & (\beta_2) & (\beta_{11}) & (\beta_{22}) & (\beta_{12}) \\ \begin{matrix} (\beta_0) \\ (\beta_1) \\ (\beta_2) \\ (\beta_{11}) \\ (\beta_{22}) \\ (\beta_{12}) \end{matrix} & \begin{bmatrix} \sigma_{\beta_0}^2 & \sigma_{\beta_0\beta_1} & \sigma_{\beta_0\beta_2} & \sigma_{\beta_0\beta_{11}} & \sigma_{\beta_0\beta_{22}} & \sigma_{\beta_0\beta_{12}} \\ \sigma_{\beta_0\beta_1} & \sigma_{\beta_1}^2 & \sigma_{\beta_1\beta_2} & \sigma_{\beta_1\beta_{11}} & \sigma_{\beta_1\beta_{22}} & \sigma_{\beta_1\beta_{12}} \\ \sigma_{\beta_0\beta_2} & \sigma_{\beta_1\beta_2} & \sigma_{\beta_2}^2 & \sigma_{\beta_2\beta_{11}} & \sigma_{\beta_2\beta_{22}} & \sigma_{\beta_2\beta_{12}} \\ \sigma_{\beta_0\beta_{11}} & \sigma_{\beta_1\beta_{11}} & \sigma_{\beta_2\beta_{11}} & \sigma_{\beta_{11}}^2 & \sigma_{\beta_{11}\beta_{22}} & \sigma_{\beta_{11}\beta_{12}} \\ \sigma_{\beta_0\beta_{22}} & \sigma_{\beta_1\beta_{22}} & \sigma_{\beta_2\beta_{22}} & \sigma_{\beta_{11}\beta_{22}} & \sigma_{\beta_{22}}^2 & \sigma_{\beta_{22}\beta_{12}} \\ \sigma_{\beta_0\beta_{12}} & \sigma_{\beta_1\beta_{12}} & \sigma_{\beta_2\beta_{12}} & \sigma_{\beta_{11}\beta_{12}} & \sigma_{\beta_{22}\beta_{12}} & \sigma_{\beta_{12}}^2 \end{bmatrix} & \end{matrix} \quad (11)$$

$$\mathbf{Y}^T = [Y_1 \ Y_2 \ Y_3 \ \dots \ Y_n],$$

$$\mathbf{X} = \begin{bmatrix} 1 & x_{11} & x_{21} & \dots & x_{k1} & x_{11}^2 & x_{21}^2 & \dots & x_{k1}^2 & (x_1 x_2)_1 & (x_1 x_3)_1 & \dots & (x_{k-1} x_k)_1 \\ 1 & x_{12} & x_{22} & \dots & x_{k1} & x_{12}^2 & x_{22}^2 & \dots & x_{k2}^2 & (x_1 x_2)_2 & (x_1 x_3)_2 & \dots & (x_{k-1} x_k)_2 \\ \vdots & \vdots & \vdots & \ddots & \vdots & \vdots & \vdots & \ddots & \vdots & \vdots & \vdots & \ddots & \vdots \\ 1 & x_{1n} & x_{2n} & \dots & x_{kn} & x_{1n}^2 & x_{2n}^2 & \dots & x_{kn}^2 & (x_1 x_2)_n & (x_1 x_3)_n & \dots & (x_{k-1} x_k)_n \end{bmatrix},$$

$$\beta^T = [\beta_0 \ \beta_1 \ \dots \ \beta_k \ \beta_{11} \ \beta_{22} \ \dots \ \beta_{kk} \ \beta_{12} \ \beta_{13} \ \dots \ \beta_{(k-1)k}]$$

This problem can be solved conceptually, by differentiating  $L$  with respect to  $\beta$ , as follows:

$$\frac{\partial L}{\partial \beta} = \frac{\partial (\mathbf{Y}^T \mathbf{Y} - \beta^T \mathbf{X}^T \mathbf{Y} - \mathbf{Y}^T \mathbf{X} \beta + \beta^T \mathbf{X}^T \mathbf{X} \beta)}{\partial \beta} = 0$$

$$= \frac{\partial (\mathbf{Y}^T \mathbf{Y} - 2\beta^T \mathbf{X}^T \mathbf{Y} + \beta^T \mathbf{X}^T \mathbf{X} \beta)}{\partial \beta} = 0$$

$$= -2\mathbf{X}^T \mathbf{Y} + 2\mathbf{X}^T \mathbf{X} \hat{\beta} = 0$$

$$\therefore \hat{\beta} = (\mathbf{X}^T \mathbf{X})^{-1} \mathbf{X}^T \mathbf{Y} \quad (7)$$

where  $\hat{\beta}$  is the estimator of the parameter  $\beta$ , obtained from experimental data.

Two properties of OLS are particularly important; they are: the expected value  $E(\hat{\beta}) = \beta$  and the covariance  $Cov(\hat{\beta}) = \sigma^2 (\mathbf{X}^T \mathbf{X})^{-1} = \tilde{\Sigma}_{\hat{\beta}}$ , where  $\sigma^2$  is the experimental variance, calculated from replicated experiments (in CCD, the values measured in the center points are used to calculate  $\sigma^2$ ). These properties can be obtained from:

$$E(\hat{\beta}) = E((\mathbf{X}^T \mathbf{X})^{-1} \mathbf{X}^T \mathbf{Y})$$

$$= (\mathbf{X}^T \mathbf{X})^{-1} \mathbf{X}^T E(\mathbf{Y})$$

$$= (\mathbf{X}^T \mathbf{X})^{-1} \mathbf{X}^T \mathbf{X} \beta = \beta \quad (8)$$

And:

$$Cov(\hat{\beta}) = E\{[\hat{\beta} - E(\hat{\beta})]^T [\hat{\beta} - E(\hat{\beta})]\}$$

$$= E\{[(\hat{\beta} - \beta)(\hat{\beta} - \beta)]\}$$

$$= E\{[(\mathbf{X}^T \mathbf{X})^{-1} (\mathbf{X}^T \varepsilon)][(\mathbf{X}^T \mathbf{X})^{-1} (\mathbf{X}^T \varepsilon)]\}$$

$$= E\{[(\mathbf{X}^T \mathbf{X})^{-1} (\mathbf{X}^T \varepsilon)][(\varepsilon^T \mathbf{X})(\mathbf{X}^T \mathbf{X})^{-1}]\}$$

$$= E\{[(\mathbf{X}^T \mathbf{X})^{-1} (\mathbf{X}^T \varepsilon)][(\varepsilon^T \varepsilon)(\mathbf{X}^T \mathbf{X})^{-1}]\}$$

$$= E(\varepsilon^T \varepsilon)(\mathbf{X}^T \mathbf{X})^{-1} = \sigma^2 (\mathbf{X}^T \mathbf{X})^{-1} = \tilde{\Sigma}_{\hat{\beta}} \quad (9)$$

For a full quadratic model with  $k = 2$ , we can write:

$$\hat{Y}(\mathbf{x}) = \hat{\beta}_0 + \hat{\beta}_1 x_1 + \hat{\beta}_2 x_2 + \hat{\beta}_{11} x_1^2 + \hat{\beta}_{22} x_2^2 + \hat{\beta}_{12} x_1 x_2 \quad (10)$$

Then:

Since  $\beta$  is estimated from the experimental data, each of its coefficients produces a component of variance for the response surface model, as shown in Eq. (11). Box and Hunter [7] advocated that, when analyzed individually, the variance of each coefficient of the response surface model brings little information about the prediction variance. Thus, a combined analysis of all the individual variances of the coefficients must be used to estimate the variance of the model. Moreover, the position of the points in the design space also induces to model variance (because only some points are measured to explore a given region of interest). Therefore, the prediction variance function is given

as follows [7,24]:

$$\begin{aligned} \text{Var}[\hat{Y}(\mathbf{x})] &= \text{Var}[(\mathbf{x}^T\boldsymbol{\beta})] \\ \text{Var}[\hat{Y}(\mathbf{x})] &= \mathbf{x}^T[\text{Var}(\boldsymbol{\beta})]\mathbf{x} \end{aligned} \tag{12}$$

Since:

$$[\text{Var}(\boldsymbol{\beta})] = \sigma^2[(\mathbf{X}^T\mathbf{X})^{-1}] \tag{13}$$

Then,

$$\text{Var}[\hat{Y}(\mathbf{x})] = \sigma^2[\mathbf{x}^{(m)T}(\mathbf{X}^T\mathbf{X})^{-1}\mathbf{x}^{(m)}] \tag{14}$$

Thus, the variance of  $\hat{Y}(\mathbf{x})$  at a given point  $\mathbf{x}_0$  of the experimental space will be given by:

$$\text{Var}[\hat{Y}(\mathbf{x})|\mathbf{x}_0] = \sigma^2[\mathbf{x}_0^{(m)T}(\mathbf{X}^T\mathbf{X})^{-1}\mathbf{x}_0^{(m)}] \tag{15}$$

For  $k = 2$ , for instance,  $\mathbf{x}_0^{(m)T} = \mathbf{x}_0^{(2)T} = [1, x_1, x_2, x_1^2, x_2^2, x_1x_2]$ .

Eq. (15) may be slightly modified to determine the confidence interval for predicting a new observation:

$$\begin{aligned} \text{Var}[Y(\mathbf{x}_0) - \hat{Y}(\mathbf{x}_0)] &= \underbrace{\text{Var}[Y(\mathbf{x}_0)]}_{\sigma^2} + \underbrace{\text{Var}[\hat{Y}(\mathbf{x}_0)]}_{\sigma^2[\mathbf{x}_0^T(\mathbf{X}^T\mathbf{X})^{-1}\mathbf{x}_0]} \\ &\quad - \underbrace{2\text{Cov}[Y(\mathbf{x}_0); \hat{Y}(\mathbf{x}_0)]}_0 \end{aligned} \tag{16}$$

We can write the variance of the difference between the new observed value and the value predicted by the model for  $\mathbf{x}_0$  as:

$$\text{Var}[Y(\mathbf{x}_0) - \hat{Y}(\mathbf{x}_0)] = \sigma^2 + \sigma^2[\mathbf{x}_0^T(\mathbf{X}^T\mathbf{X})^{-1}\mathbf{x}_0] = \sigma^2\{1 + [\mathbf{x}_0^T(\mathbf{X}^T\mathbf{X})^{-1}\mathbf{x}_0]\} \tag{17}$$

Thus, the confidence interval of the predicted value for a new observation will be:

$$E(Y|\mathbf{x}_{new}) = \hat{Y}(\mathbf{x}_{new}) \pm t_{\alpha/2; n-p} \times s\sqrt{1 + \mathbf{x}_{new}^T(\mathbf{X}^T\mathbf{X})^{-1}\mathbf{x}_{new}} \tag{18}$$

In Eq. (18),  $s$  represents the estimate of  $\sigma$  and can be given by  $s = \sqrt{\frac{\sum_{i=1}^n \varepsilon_i^2}{n-p}}$ , where  $\sum_{i=1}^n \varepsilon_i^2 = SS_E$  is the error sum of squares,  $n$  is the number of observations, and  $p$  is the number of parameters. Considering the properties of the CCD,  $SS_E$  can be obtained with the responses measured at the center points.

Based on the idea of prediction variance, Box and Draper [24] proposed the Scaled Prediction Variance (SPV) function for (1) assessment of individual design performance and (2) standardized comparison of competing designs. The SPV is given by:

$$V(\mathbf{x}) = \frac{N}{\sigma^2} \text{Var}[\hat{Y}(\mathbf{x})] \tag{19}$$

Since:

$$\text{Var}[\hat{Y}(\mathbf{x})] = \sigma^2[\mathbf{x}_0^T(\mathbf{X}^T\mathbf{X})^{-1}\mathbf{x}_0] \tag{20}$$

Then:

$$\begin{aligned} V(\mathbf{x}) &= \frac{N}{\sigma^2} \sigma^2[\mathbf{x}_0^T(\mathbf{X}^T\mathbf{X})^{-1}\mathbf{x}_0] \\ V(\mathbf{x}) &= N[\mathbf{x}_0^T(\mathbf{X}^T\mathbf{X})^{-1}\mathbf{x}_0] \end{aligned} \tag{21}$$

Originally, Box and Draper [24] proposed the scaling of the prediction variance function by the term  $N/\sigma^2$  as a way of providing a standardized measure of the variance of the designs, since: (1) for the same experiment,  $\sigma^2$  is expected constant regardless of the design chosen, so it can be eliminated, and (2) with the inclusion of experimental points,  $(\mathbf{X}^T\mathbf{X})^{-1}$  is reduced at least in some design region, so  $N$  is added as a compensation factor. In practical terms, the multiplication of the prediction variance function by  $N$  is known as a cost penalty factor [25–27], that is, the fewer experiments required to reduce variance, the lower the SPV and, consequently, the better the experimental design.

Fig. 1 presents the profiles of the SPV function for a two-factor CCD with 4 factorial points, 4 axial points and different amounts of center points. As can be seen in the figure, the lower the number of center

points, the greater the SPV in the design center and the greater its irregularities. On the other hand, the higher the number of center points, the smoother the SPV becomes from the design center.

For the same experimental design, the scaling of the SPV function by  $N$  does not affect the behavior of the variance along the design space. Thus, a more direct measure of the variance provoked by the design structure along the experimental region can be obtained by eliminating  $N$  [27]:

$$\frac{V(\mathbf{x})}{N} = [\mathbf{x}_0^T(\mathbf{X}^T\mathbf{X})^{-1}\mathbf{x}_0] \tag{22}$$

If we want to obtain a direct measure of the precision of the model at a given point in the design, then the variance of the observations must also be considered [28], which leads back to Eq. (15).

### 3. Process capability analysis

Process capability analyses seek to evaluate the behavior of the process variability with respect to the allowed variability. Conceptually, a process is capable when it generates products within the specification limits, that is when there are no nonconforming products [29]. In practice, for the evaluation of the capability or performance of a process, several indices may be employed [30], called capability ratios if the process is under statistical control (there are only natural causes of variation) or performance indexes if the process is not under statistical control (there are also special causes of variation) [29]. The use of the capability ratios is often considered more appropriate for the investigation of a process since it is assumed that special causes such as defects in machine components or damaged tools have already been eliminated [31].

The index  $C_p$  is defined as the ratio of the total variability allowed, measured by the difference between the specification limits, to the natural variability of the process, measured by six standard deviations (a common assumption is that the data comes from a normal distribution):

$$C_p = \frac{(USL - LSL)}{6\sigma} \tag{23}$$

where USL and LSL represent the upper and the lower limits, respectively, and  $\sigma$  represent the process standard deviation.

The confidence interval of  $C_p$  is given by:

$$\hat{C}_p \sqrt{\frac{(\chi^2_{1-\alpha/2; n-1})}{n-1}} \leq C_p \leq \hat{C}_p \sqrt{\frac{(\chi^2_{\alpha/2; n-1})}{n-1}} \tag{24}$$

where  $\hat{C}_p$  is the estimator of the parameter  $C_p$ , obtained from experimental data,  $\chi^2$  is the Chi-Squared statistic evaluated for a given significance level  $\alpha$  and  $n - 1$  degrees of freedom (which only depends on the number of observations  $n$ ).

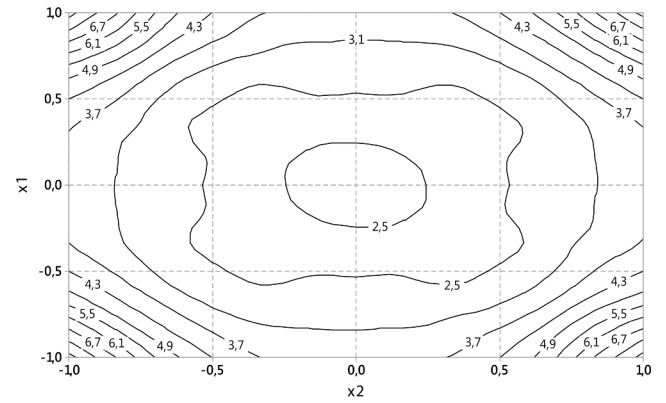
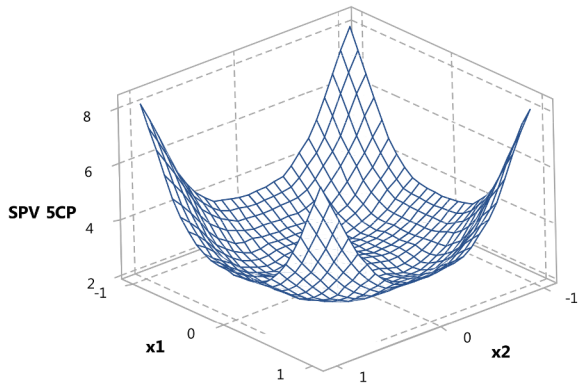
Although it is an easily obtainable index,  $C_p$  is not sensitive to displacements in the process mean. Fig. 2 illustrates some cases where the same  $C_p$  is observed for five processes under different conditions of centrality. For these cases, other capability ratios are more appropriate, such as the indices  $C_{pk}$  and  $C_{pm}$ .

The index  $C_{pk}$  is defined as the minimum of the unilateral capability ratios  $C_{pl}$  and  $C_{pu}$ , as shown in Eqs. (25)-(27). The idea is that, since the standard deviation  $\sigma$  is the same for both ratios, the minimum will provide the process capability with respect to the limit closest to the process mean (worst case scenario). If the process is capable in this scenario, it will also be capable in the other scenario and vice versa.

$$C_{pl} = \frac{(\mu - LSL)}{3\sigma} \tag{25}$$

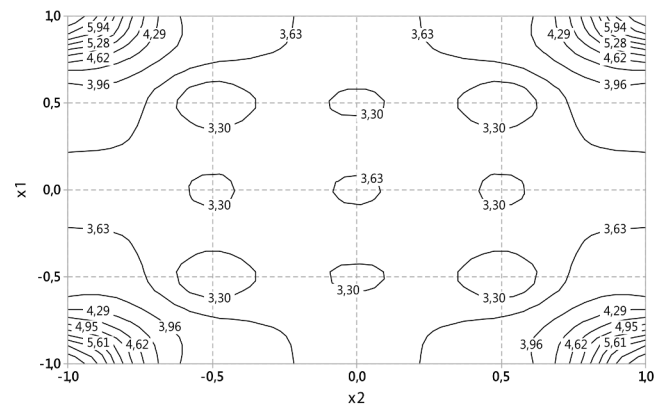
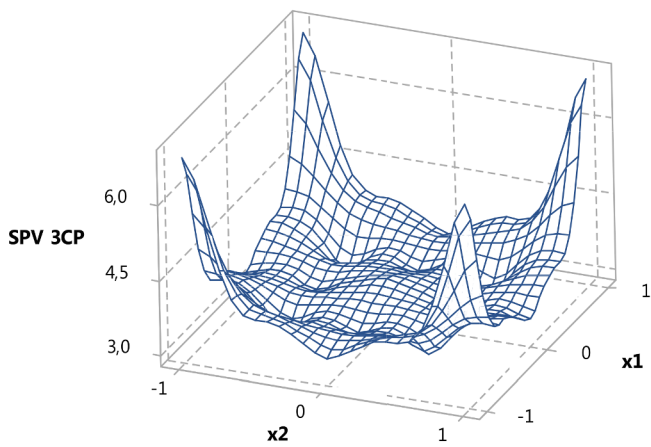
$$C_{pu} = \frac{(USL - \mu)}{3\sigma} \tag{26}$$

Contour Plot of SPV 5CP vs x1; x2



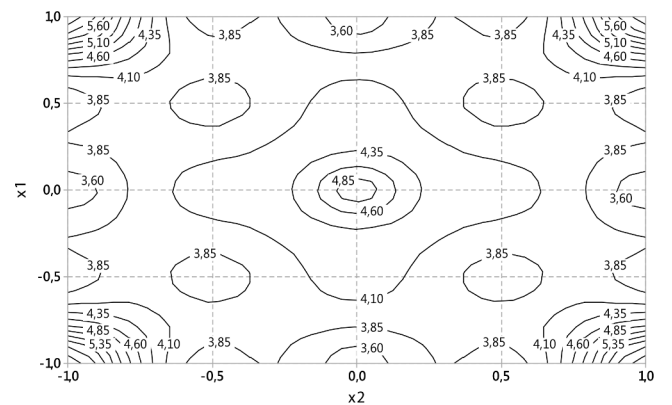
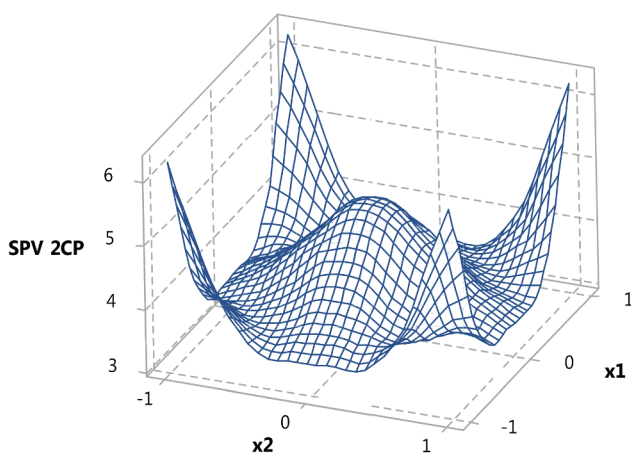
(a)

Contour Plot of SPV 3CP vs x1; x2



(b)

Contour Plot of SPV 2CP vs x1; x2



(c)

Fig. 1. Scale Prediction Variance for different amounts of center points: a) five center point, b) three center points and c) two center points.

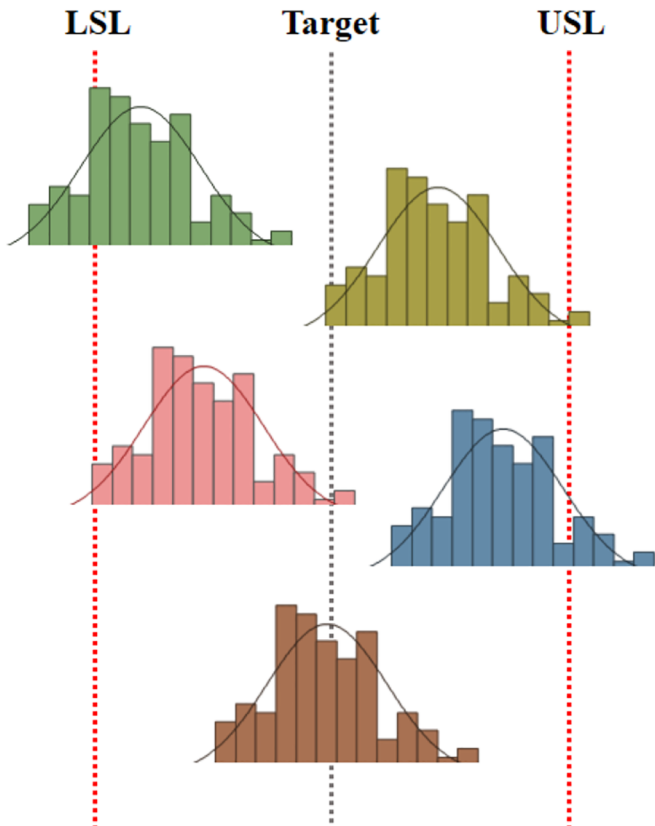


Fig. 2. Processes under different conditions of centrality with the same  $C_p$ .

**Table 2**  
Recommended minimum values of the capability ratio.  
Source: Montgomery [29].

	Two-sided specifications	One-sided specifications
Existing processes	1.33	1.25
New processes	1.50	1.45
Safety, strength, or critical parameter, existing process	1.50	1.45
Safety, strength, or critical parameter, new process	1.67	1.60

$$C_{pk} = \text{Min} \left\{ \frac{(\mu - LSL)}{3\sigma}, \frac{(USL - \mu)}{3\sigma} \right\} \tag{27}$$

where  $\mu$  represents the process mean.

The confidence interval of  $C_{pk}$  is given by:

$$\hat{C}_{pk} \left[ 1 - Z_{\alpha/2} \sqrt{\frac{1}{9n\hat{C}_{pk}^2} + \frac{1}{2(n-1)}} \right] \leq C_{pk} \leq \hat{C}_{pk} \left[ 1 + Z_{\alpha/2} \sqrt{\frac{1}{9n\hat{C}_{pk}^2} + \frac{1}{2(n-1)}} \right] \tag{28}$$

If the mean does not coincide with the centrality target  $T$  of the process, other measures become more suitable. The ratio  $C_{pm}$ , for instance, includes the displacement of the process mean to the target  $T$  as a second component of process variability:

$$C_{pm} = \frac{USL - LSL}{6\sqrt{(\mu - T)^2 + \sigma^2}} \tag{29}$$

A process is said to be capable if the capability ratio is greater than acceptability levels. Table 2 summarizes the recommended minimum

values according to Montgomery [29]. Although there is no consensus on these values [32,33], the approach proposed by Montgomery [29] has the advantage of establishing the minimum values regarding the condition of the process and the number of specification limits.

#### 4. Multiobjective optimization

Industrial processes, by their very nature, have multiple dimensions of interest, often divided into critical-to-quality (CTQ) and critical-to-performance (CTP) characteristics. This implies that optimization problems will most often be multiobjective with conflicting objectives since the gain in one characteristic usually implies a loss in another and vice versa.

To address multiobjective problems where there is a trade-off between the characteristics of interest, the Weighted Sums (WS) method is one of the most commonly used. This technique consists of an agglutination operator, in which the functions of interest are weighted to establish the degree of the relative importance of each function. The method solves a sequence of subproblems from the minimization of a global function, usually formed as a linear combination of the original variables. The result of this process is the so-called Pareto frontier, where the set of solutions is presented as ordered pairs of the objective functions. Given the original functions  $f_i(x)$  and weights  $w_i \geq 0$ , with  $i = 1, 2, \dots, m$ , the multiobjective problem via WS method is formulated according to Eq. (30):

$$\begin{aligned} \min_x \quad & \sum_{i=1}^n w_i f_i(x) = \mathbf{w}^T \mathbf{F}(x) \\ \text{s. t.} \quad & x \in C \end{aligned} \tag{30}$$

The Global Criterion Method (GCM) is another conventional multiobjective technique, which uses a global agglutination operator of the standardized distances of the functions to their reference values [34]. In this method, the optimization is performed by minimizing the global function for different weights  $w_i \geq 0$ , with  $i = 1, 2, \dots, m$ , according to Eq. (31):

$$\begin{aligned} \min_x \quad & \sum_{i=1}^n w_i \left[ \frac{f_i(x) - f_i^U}{f_i^U} \right] = \mathbf{w}^T \mathbf{F}_{\text{GCM}}(x) \\ \text{s. t.} \quad & x \in C \end{aligned} \tag{31}$$

where  $f_i^U$  is the individual optimal of the  $i$ th function.

If the original functions have different convexities, the frontier becomes non-convex and discontinuous with the traditional approaches, forming clusters of Pareto-optimal solutions in some regions, but discontinuous in the solution space. To overcome these problems, Das and Dennis [35] proposed the Normal Boundary Intersection (NBI) method, showing that this technique is able to produce Pareto frontiers evenly distributed, independent of the convexities of the functions and their relative scales. Many studies have demonstrated the effectiveness of the NBI method for process optimization.

Brito et al. [36] studied the surface roughness in the end milling process of AISI 1045 steel by using Robust Parameter Design (RPD). The authors applied both the NBI and the WS methods to minimize the Multivariate Mean Square Error (MMSE) for  $Ra$ ,  $Rt$  and their variances. They concluded that in regions where the WS-MMSE method revealed discontinuities, the NBI-MMSE method was able to find feasible solutions.

Similar conclusions were drawn by Costa et al. [37], who performed the optimization of five responses of surface roughness (quality measures) and one response of material removal rate (MRR; performance measure) for the dry end milling process of AISI 1045 steel. The authors used the Principal Component Analysis (PCA) and the MMSE to reduce the dimensionality of the problem and extract the correlation between the original responses. As a result of the optimization, they observed that the proposed NBI-PCA-MMSE method overcame the WS-PCA-MMSE method, showing that the NBI-based method was the only able to generate a Pareto frontier with equispaced points.

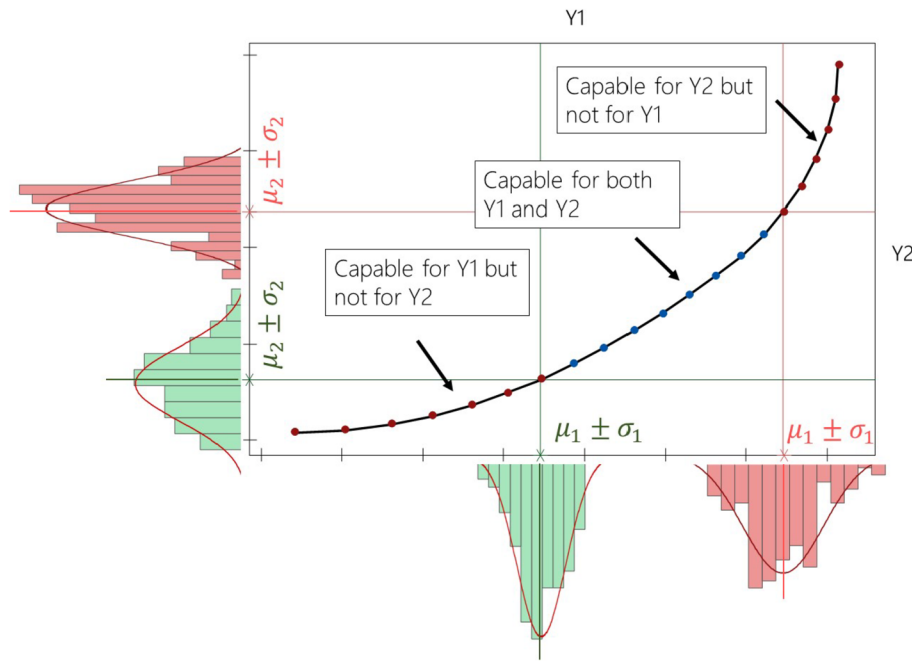


Fig. 3. Prediction capability regions for Pareto optimal solutions. Note: The two selected points delimit the capable region for both response variables.

Liu et al. [38] showed that the NBI was more favorable than the convex WS method for the maximization of productivity and minimization of consumption for a biotechnological fed-batch process, concluding that the NBI method provides a more accurate representation of Pareto set. Differently from Brito et al. [36] and Costa et al. [37] that minimized all the latent MMSE functions, Liu et al. [38] optimized responses with different optimization directions; even, in this case, the NBI was more satisfactory.

Gaudencio et al. [34] proposed the optimization of turning process of the AISI H13 hardened steel by using a fuzzy NBI-MMSE. The authors demonstrated that the proposed method presented a better performance in the construction of the Pareto frontier in comparison to three other methods: WS-MMSE, Global Criterium Method (GCM)-MMSE, and Arc homotopic length (AHL)-MMSE.

Recently, a method comparable to the NBI, called Normalized Normal Constraint (NNC), has also become popular for finding evenly distributed Pareto frontiers. In essence, the NNC combines the original fundamentals of the NBI with the  $\epsilon$ -constraint method, by employing inequality constraints to iteratively reduce the feasible objective space and, therefore, find the optimal points. Detailed explanations about the NNC method can be found in Messac et al. [39] and Logist et al. [40].

### 5. Multi-criteria optimization based on capability ratios

In this section, a multi-criteria optimization based on capability ratios strategy is developed.

#### 5.1. The problem

Considering the stochastic nature of the processes, in this work, we approach three problems faced by the experimenter:

(1) First, the experimenter seeks optimal solutions to the process investigated from the optimization of a set of responses of interest; however, from a practical point of view, the concept of optimality is often used only for mean values of the responses, ignoring the components of variance and, therefore, the stochastic nature of the processes. As a consequence, although the means are optimized, in many cases the presence of high variability prevents real

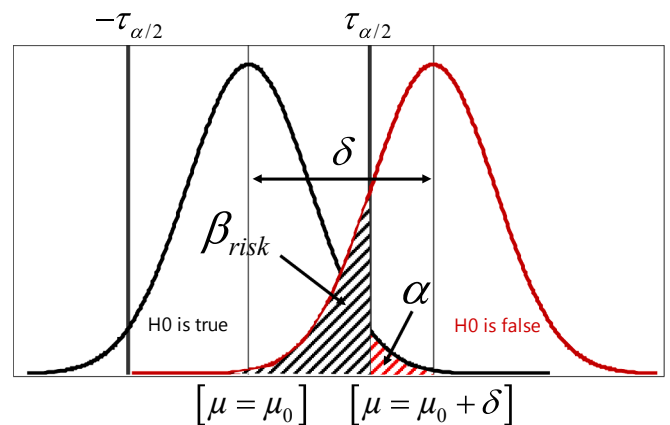


Fig. 4. Probability of the type II error for Pareto solutions.

improvements from being observed in practice. Moreover, since the industrial processes optimized normally intend to produce thousands (sometimes millions) of products, large amounts of variability can imply in non-conformities and inefficiencies. As discussed in Section 2, we know that the regression models are affected both by experimental data error and design variance. Then, the experimenter should also take into consideration the model variance in the process optimization problem.

- (2) In multi-criteria problems, there is another problem. Since the optimal solutions are combinations of the original response variables, each model can present different prediction capabilities. Therefore, for many “optimal solutions”, the combined prediction capability can be unsatisfactory. Fig. 3 illustrates different levels of model capabilities for the bidimensional case. The key idea is that the Pareto optimal solutions can be distributed into three capability clusters: (1) capable for Y1 but not for Y2, (2) capable for both Y1 and Y2, and (3) capable for Y2 but not for Y1.
- (3) Finally, there is a third problem. Although Pareto frontier contains several optimal combinations of the original responses, the presence of variability may make some of these solutions indistinguishable [41,42] or, in other words, dependent on very large

confirmatory sample sizes for differences to be detected. Depending on process variability, design point, and conflict relationship between response variables, this can occur even in capable regions.

Fig. 4 shows that the distributions of two different points of Pareto frontier can be confused, with a given probability  $\beta_{risk}$ . This probability denotes the type II error and depends especially on the variance of the Pareto frontier points, the difference to be detected between them and the sample size used to estimate the bilateral test statistics  $-\tau_{\alpha/2}$  and  $\tau_{\alpha/2}$ . The greater the  $\beta_{risk}$ , the smaller the chance of the number of points on the Pareto frontier to be equivalent to the number of solutions observed in practice, although this also depends on the spacing used for discretization of the Pareto points.

### 5.2. Boundary conditions

To formulate the optimization model, we assume the following boundary conditions:

- (1) The original response variables are linearly independent ( $\rho_{y_1, y_2} \cong 0$ ).
- (2) The measurement system (MS) is appropriate for measuring the original responses, which implies that the MS does not increase the data variance ( $\sigma_{gage}^2 \cong 0$ ) and there is no measurement bias.
- (3) The polynomial models estimated are appropriate for representing the regions of interest of each response variable, which implies that the model does not contain estimation bias ( $B \cong 0$ ).
- (4) The process mean matches the target ( $\mu - T \cong 0$ ).
- (5) In the design space, the process is not sensitive to disturbances due to noise variables ( $\sigma_z^2 \cong 0$ )

### 5.3. Process optimization model

The objective of the proposed model is to simultaneously optimize the original process variables, at the same time that the variances of the regression models are minimized. Due to the nature of each response, the estimated regression models present different variances. Therefore, we propose that the variance of each model be embedded in its expected value, transforming the multi-criteria optimization with  $n$  objective functions ( $n/2$  means and  $n/2$  variances) into a problem with  $n/2$  latent objective functions. However, care must be taken when combining expected value and variance, since this combination can increase the non-linearity of the problem, reducing the effectiveness of some search algorithms, such as the GRG. For this, in this work, we have developed an optimization strategy where the variances of the models are used as components of variability of the capability ratio  $C_{pk}$ , while at the same time the nadir points are used as specification limits. The development of the optimization model follows the stages below:

- (1) We propose a modified  $C_{pk}(\mathbf{x})$  as a measure of model-process capability. In the proposed  $C_{pk}(\mathbf{x})$ , the mean is the expected value  $E[Y(\mathbf{x})]$  of the response of interest and the variance is a combination of experimental error  $\sigma_{f(\mathbf{x})}$  and design prediction variance  $V(\mathbf{x})$ , called model variance  $Var[Y(\mathbf{x})|\mathbf{x}_0]$ , as presented in Eq. (15) – Section 2. The proposed  $C_{pk}(\mathbf{x})$  is given by the following expression:

$$C_{pk}(\mathbf{x}) = \min(C_{pu}, C_{pl})$$

$$= \min\left\{\frac{USL - E[Y(\mathbf{x})]}{3 \cdot \sqrt{Var[Y(\mathbf{x})|\mathbf{x}_0]}}, \frac{E[Y(\mathbf{x})] - LSL}{3 \cdot \sqrt{Var[Y(\mathbf{x})|\mathbf{x}_0]}}\right\}$$

$$= \min\left\{\frac{USL - E[Y(\mathbf{x})]}{3 \cdot \sigma_{f_i(\mathbf{x})} \sqrt{[x_0^{(m)T} (\mathbf{X}^T \mathbf{X})^{-1} x_0^{(m)}]}}, \frac{E[Y(\mathbf{x})] - LSL}{3 \cdot \sigma_{f_i(\mathbf{x})} \sqrt{[x_0^{(m)T} (\mathbf{X}^T \mathbf{X})^{-1} x_0^{(m)}]}}\right\} \quad (32)$$

Considering that  $Y(\mathbf{x})$  has a defined optimization direction,  $C_{pk}(\mathbf{x})$  will have an unilateral specification limit; therefore, if  $Y(\mathbf{x})$  must be minimized, then  $C_{pk}(\mathbf{x}) = C_{pu}$  and if  $Y(\mathbf{x})$  must be maximized, then  $C_{pk}(\mathbf{x}) = C_{pl}$ .

- (2) For both cases (minimization or maximization of  $Y(\mathbf{x})$ ), we propose the individual Nadir solution of the original response variables as the specification limit, since it is the worst solution for the investigated response but implies that at least one other response reaches its best solution. Then, the individual Nadir solution is the natural limit for the responses used in the multi-criteria optimization, because values less (maximization problem) or greater (minimization problem) than it do not improve the other responses. Moreover, values greater (maximization problem) or less (minimization problem) than individual Nadir solution imply the reduction of the solution space. Therefore:

- If  $Y(\mathbf{x})$  must be minimized:

$$C_{pk}^i(\mathbf{x}) = \frac{USL - E[Y_i(\mathbf{x})]}{3 \cdot \sqrt{Var[Y_i(\mathbf{x})|\mathbf{x}_0]}} = \frac{[f_i^N - f_i(\mathbf{x})]}{3 \cdot \sigma_{f_i(\mathbf{x})} \sqrt{[x_0^{(m)T} (\mathbf{X}^T \mathbf{X})^{-1} x_0^{(m)}]}}$$

for  $i = 1, 2, \dots, m$  (33)

- If  $Y(\mathbf{x})$  must be maximized:

$$C_{pk}^i(\mathbf{x}) = \frac{E[Y_i(\mathbf{x})] - LSL}{3 \cdot \sqrt{Var[Y_i(\mathbf{x})|\mathbf{x}_0]}} = \frac{[f_i(\mathbf{x}) - f_i^N]}{3 \cdot \sigma_{f_i(\mathbf{x})} \sqrt{[x_0^{(m)T} (\mathbf{X}^T \mathbf{X})^{-1} x_0^{(m)}]}}$$

for  $i = 1, 2, \dots, m$  (34)

- (3) Now, considering the capability ratios  $C_{pk}^i(\mathbf{x})$  as objective functions, the multi-criteria optimization problem is formulated as follows:

$$\max_{\mathbf{x}} C_{pk}(\mathbf{x}) = [C_{pk}^1(\mathbf{x}), \dots, C_{pk}^i(\mathbf{x}), \dots, C_{pk}^m(\mathbf{x})]$$

s.t.:  $\mathbf{x}^T \mathbf{x} \leq \rho^2$  (35)

- (4) To solve the multi-criteria problem formulated in stage (3), we proposed the Normal Boundary Intersection (NBI) method, since this technique produces Pareto frontiers evenly distributed, independent of the convexities of the functions and their relative scales [35]. In this method, the first step is to build the payoff matrix  $\Phi$ . This matrix can be obtained by the individual optimization of each objective function. In matrix notation,  $\Phi$  can be written as:

$$\Phi = \begin{bmatrix} f_1^*(x_1^*) & \dots & f_1(x_i^*) & \dots & f_1(x_m^*) \\ \vdots & \ddots & \vdots & \ddots & \vdots \\ f_i(x_1^*) & \dots & f_i^*(x_i^*) & \dots & f_i(x_m^*) \\ \vdots & \ddots & \vdots & \ddots & \vdots \\ f_m(x_1^*) & \dots & f_m(x_i^*) & \dots & f_m^*(x_m^*) \end{bmatrix} \quad (36)$$

where  $x_m^*$  denotes the “optimum” of a given function  $m$ ,  $f_m^*(x_m^*)$  denotes the “optimal” function  $m$  evaluated with respect to its optimum  $x_m^*$ , and  $f_i(x_m^*)$  denotes the  $i$ th function evaluated with respect to the optimum  $x_m^*$  [43].

The set of individual optimal solutions is given in the main diagonal of  $\Phi$  and form the Utopia point  $f^U = [f_1^*(x_1^*), \dots, f_i^*(x_i^*), \dots, f_m^*(x_m^*)]$ . In general, this point lies outside the feasible region and represents the idealized solution, where all the objective functions reach their best values. On the other hand, the set of individual worst solutions form the Nadir point  $f^N = [f_1^N, \dots, f_i^N, \dots, f_m^N]$ , which represents the scenario where all the objective functions fail in providing optimal solutions. We can obtain the individual Nadir solution of a function  $f_m$  when evaluating  $f_m$  with respect to the individual optima  $x_1^*, \dots, x_i^*, \dots, x_{m-1}^*$  of  $f_1, \dots, f_i, \dots, f_{m-1}$ , respectively. The individual Nadir solution of  $f_m$  will be the worst value of this set.

The Nadir and Utopia points are used to normalize the original functions, as shown in Eq. (37):

$$\bar{f}_i(\mathbf{x}) = \left[ \frac{f_i(\mathbf{x}) - f_i^U}{f_i^U - f_i^N} \right], \quad i = 1, 2, \dots, m \quad (37)$$

From this transformation, both a normalized payoff matrix  $\bar{\Phi}$  and a

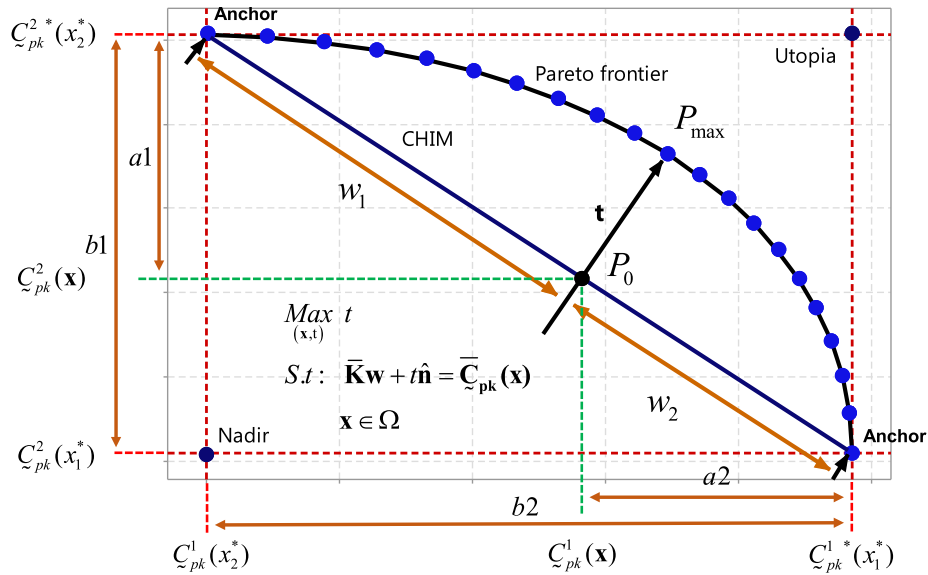


Fig. 5. NBI-GRG method: Pareto frontier for capability ratios maximization.

normalized vector of objective functions  $\bar{F}(x)$  can be obtained.

$$\bar{\Phi} = \begin{bmatrix} \bar{f}_1^*(x_1^*) & \dots & \bar{f}_1(x_1^*) & \dots & \bar{f}_1(x_m^*) \\ \vdots & \ddots & \vdots & \ddots & \vdots \\ \bar{f}_i^*(x_1^*) & \dots & \bar{f}_i^*(x_i^*) & \dots & \bar{f}_i(x_m^*) \\ \vdots & \ddots & \vdots & \ddots & \vdots \\ \bar{f}_m^*(x_1^*) & \dots & \bar{f}_m(x_i^*) & \dots & \bar{f}_m^*(x_m^*) \end{bmatrix}, \bar{F}(x) = \begin{bmatrix} \bar{f}_1(x_1) \\ \vdots \\ \bar{f}_i(x_i) \\ \vdots \\ \bar{f}_m(x_m) \end{bmatrix} \quad (38)$$

Since  $C_{pk}^i(x)$  is desired to be maximized, the payoff matrix  $K$  of the proposed problem is obtained by individual maximization of each  $C_{pk}^i(x)$ :

$$\begin{aligned} & \max_x C_{pk}^i(x) \\ & \text{s.t.: } x^T x \leq \rho^2 \\ & \begin{bmatrix} C_{pk}^1(x) \\ \vdots \\ C_{pk}^i(x) \\ \vdots \\ C_{pk}^m(x) \end{bmatrix} \geq \begin{bmatrix} 0 \\ \vdots \\ 0 \\ \vdots \\ 0 \end{bmatrix}, i = 1, 2, \dots, m \end{aligned} \quad (39)$$

Substituting the values in the matrix presented in Eq. (36), we found:

$$K = \begin{bmatrix} C_{pk}^{1*}(x_1^*) & \dots & C_{pk}^1(x_i^*) & \dots & C_{pk}^1(x_m^*) \\ \vdots & \ddots & \vdots & \ddots & \vdots \\ C_{pk}^i(x_1^*) & \dots & C_{pk}^{i*}(x_i^*) & \dots & C_{pk}^i(x_m^*) \\ \vdots & \ddots & \vdots & \ddots & \vdots \\ C_{pk}^m(x_1^*) & \dots & C_{pk}^m(x_i^*) & \dots & C_{pk}^{m*}(x_m^*) \end{bmatrix} \quad (40)$$

Given these formulations, we can revisit stage (2), noting that the optimization problem presented in Eq. (39) is one more practical argument for using the Nadir points as specification limits, since in practice, as  $C_{pk}^i(x)$  will be maximized for all  $i > 0$ , and for the sake of simplicity we consider process variables with always positive measures, then the individual optimizations of Eq. (39) provide the relation of greater distance to Nadir points of the original variables (also combined with the smaller model variance).

Using the original concept of the NBI method, we can obtain a convenient transformation for  $C_{pk}^i(x)$ . Fig. 5 presents the Pareto frontier for capability ratios maximization. From this figure, we deduce the following relations:

$$\begin{aligned} \frac{a_1}{b_1} &= \frac{C_{pk}^{2*}(x_2^*) - C_{pk}^2(x)}{C_{pk}^{2*}(x_2^*) - C_{pk}^2(x_1^*)} = \frac{w_2}{w_1 + w_2} = \frac{C_{pk}^{iU} - C_{pk}^i(x)}{C_{pk}^{iU} - C_{pk}^{iN}} = \frac{C_{pk}^i(x) - C_{pk}^{iU}}{C_{pk}^{iN} - C_{pk}^{iU}} \\ &= \bar{C}_{pk}^i(x_i) \end{aligned} \quad (41)$$

$$\begin{aligned} \frac{a_2}{b_2} &= \frac{C_{pk}^{1*}(x_1^*) - C_{pk}^1(x)}{C_{pk}^{1*}(x_1^*) - C_{pk}^1(x_2^*)} = \frac{w_2}{w_1 + w_2} = \frac{C_{pk}^{iU} - C_{pk}^i(x)}{C_{pk}^{iU} - C_{pk}^{iN}} = \frac{C_{pk}^i(x) - C_{pk}^{iU}}{C_{pk}^{iN} - C_{pk}^{iU}} \\ &= \bar{C}_{pk}^i(x_i) \end{aligned} \quad (42)$$

Therefore:

$$\begin{aligned} C_{pk}^2(x) &= C_{pk}^{2*}(x_2^*) + w_1 C_{pk}^2(x_1^*) - w_1 C_{pk}^{2*}(x_2^*) \\ &= w_1 C_{pk}^2(x_1^*) + (1 - w_1) C_{pk}^{2*}(x_2^*) = w_1 C_{pk}^2(x_1^*) + w_2 C_{pk}^{2*}(x_2^*) \end{aligned} \quad (43)$$

$$\begin{aligned} C_{pk}^1(x) &= C_{pk}^{1*}(x_1^*) + w_2 C_{pk}^1(x_2^*) - w_2 C_{pk}^{1*}(x_1^*) \\ &= w_2 C_{pk}^1(x_2^*) + (1 - w_2) C_{pk}^{1*}(x_1^*) = w_1 C_{pk}^{1*}(x_1^*) + w_2 C_{pk}^1(x_2^*) \end{aligned} \quad (44)$$

In the matrix notation, the equations representing the coordinates of the point  $P_0$  and  $P_{max}$  can be written as:

$$\begin{cases} C_{pk}^1(x) = w_1 C_{pk}^{1*}(x_1^*) + w_2 C_{pk}^1(x_2^*) \\ C_{pk}^2(x) = w_1 C_{pk}^2(x_1^*) + w_2 C_{pk}^{2*}(x_2^*) \end{cases} \quad (45)$$

$$\begin{bmatrix} C_{pk}^1(x) \\ C_{pk}^2(x) \end{bmatrix}_{\bar{C}_{pk}(x)} = \begin{bmatrix} C_{pk}^{1*}(x_1^*) & C_{pk}^1(x_2^*) \\ C_{pk}^2(x_1^*) & C_{pk}^{2*}(x_2^*) \end{bmatrix}_K \times \begin{bmatrix} w_1 \\ w_2 \end{bmatrix}_w \quad (46)$$

$$\bar{C}_{pk}(x) = Kw \quad (47)$$

Then, by applying Eqs. (41)-(47), we obtain the normalized payoff matrix and the normalized vector of objective capability functions:

$$\bar{K} = \begin{bmatrix} \bar{C}_{pk}^{1*}(x_1^*) & \dots & \bar{C}_{pk}^1(x_i^*) & \dots & \bar{C}_{pk}^1(x_m^*) \\ \vdots & \ddots & \vdots & \ddots & \vdots \\ \bar{C}_{pk}^i(x_1^*) & \dots & \bar{C}_{pk}^{i*}(x_i^*) & \dots & \bar{C}_{pk}^i(x_m^*) \\ \vdots & \ddots & \vdots & \ddots & \vdots \\ \bar{C}_{pk}^m(x_1^*) & \dots & \bar{C}_{pk}^m(x_i^*) & \dots & \bar{C}_{pk}^{m*}(x_m^*) \end{bmatrix}, \bar{C}_{pk}(x) = \begin{bmatrix} \bar{C}_{pk}^1(x_1) \\ \vdots \\ \bar{C}_{pk}^i(x_i) \\ \vdots \\ \bar{C}_{pk}^m(x_m) \end{bmatrix} \quad (48)$$

The classic NBI formulation is written as  $t$  maximization:

$$\begin{aligned}
 & \text{Max}_{(x,t)} t \\
 & \text{s. t. : } \bar{\Phi} \mathbf{w} + t \hat{\mathbf{n}} = \bar{\mathbf{F}}(\mathbf{x}) \\
 & \mathbf{x} \in \Omega \\
 & g_j(\mathbf{x}) \leq 0 \\
 & h_j(\mathbf{x}) = 0
 \end{aligned} \tag{49}$$

Replacing  $\bar{\Phi}$  by  $\bar{\mathbf{K}}$  and  $\bar{\mathbf{F}}(\mathbf{x})$  by  $\bar{\mathbf{C}}_{pk}(\mathbf{x})$  in the previous equation, we obtain the NBI bi-objective problem for model capability optimization as follows:

$$\begin{aligned}
 & \text{Max}_{(x,t)} t \\
 & \text{s. t. : } \bar{\mathbf{K}} \mathbf{w} + t \hat{\mathbf{n}} = \bar{\mathbf{C}}_{pk}(\mathbf{x}) \\
 & \mathbf{x} \in \Omega \\
 & g_j(\mathbf{x}) \leq 0 \\
 & h_j(\mathbf{x}) = 0
 \end{aligned} \tag{50}$$

Then, the equivalent problem is derived:

$$\begin{aligned}
 & \text{Min}_{\mathbf{x}} F(\mathbf{x}) = \bar{\mathbf{C}}_{pk}^1(\mathbf{x}) \\
 & \text{s. t. : } \bar{\mathbf{C}}_{pk}^1(\mathbf{x}) - \bar{\mathbf{C}}_{pk}^2(\mathbf{x}) + 2w - 1 = 0 \\
 & \mathbf{x} \in \Omega \\
 & g_j(\mathbf{x}) = \mathbf{x}^T \mathbf{x} - \rho^2 \leq 0 \\
 & h_{j+1}(\mathbf{x}) = 0
 \end{aligned} \tag{51}$$

The full demonstration can be found in Appendix A.

- (6) The Pareto frontier is generated by solving the NBI problem iteratively for different weights  $w$ . In this step, we propose the use of Generalized Reduced Gradient (GRG) algorithms as the subroutine for NBI, since the existing literature has shown that GRG is one of the most robust and efficient gradient algorithms for this proposal [37,44] and it is also available in modern computational environments, such as MS Excel [45].
- (7) After optimization, the prediction capability regions are identified in the Pareto frontier by considering appropriate limits. Considering that the original responses have one-sided specifications, we adopt the recommended minimum value for safety, strength, or critical

parameter and new process proposed by Montgomery [29]:  $\bar{\mathbf{C}}_{pk}^i(x_i) > 1.60$  (see Table 2).

- (8) Then, we propose the analysis of the risk that the selected solution is statistically equivalent to its adjacent solutions. We advocate that the decision maker can choose the levels of  $\beta_{risk}$  and the desired difference (in standard deviation terms) between the distributions of the Pareto solutions to obtain the sample sizes for confirmatory experiments. This decision can be performed on the basis of the following risk probability:

$$\beta_{risk} = \Phi\left(Z_{\alpha/2} - \frac{\delta\sqrt{n}}{\sigma_{pred}}\right) - \Phi\left(-Z_{\alpha/2} - \frac{\delta\sqrt{n}}{\sigma_{pred}}\right) \tag{52}$$

where  $\Phi$  is the probability operator,  $\delta$  is the difference between adjacent Pareto solutions, and  $\sigma_{pred}$  is the prediction standard deviation.

For the evaluation of the prediction standard deviation  $\sigma_{pred}$  of the proposed  $\bar{\mathbf{C}}_{pk}(\mathbf{x})$ , we propose the following formulation:

$$[SD(\bar{\mathbf{C}}_{pk}(\mathbf{x}))] = \sqrt{\frac{1}{9} + \frac{d^2}{54(N-1)\sigma^2 \mathbf{x}_0 (\mathbf{X}^T \mathbf{X})^{-1} \mathbf{x}_0}} \tag{53}$$

where  $d = USL - f(x)$  or  $d = f(x) - LSL$ , and  $N$  is the number of experimental data.

Full demonstrations of Eqs. (52) and (53) can be found in Appendices B and C, respectively.

Fig. 6 illustrates the practical meaning of the proposed analysis. At a given level of risk, considering the difference between the mean values of the solutions and the prediction standard deviation at the design points investigated, the solutions can rely on the same confidence region (Fig. 6a) or in independent regions (Fig. 6b). This means that the decision maker can consider both solutions 1 and 2 feasible (or infeasible) for a certain goal, but need to make separate analyses for solutions 3 and 4.

### 6. Case study

To assess the feasibility of the optimization strategy proposed in section 5.3 as a suitable optimization for multi-criteria response surface problems, in this section, we illustrate the presented formulations by

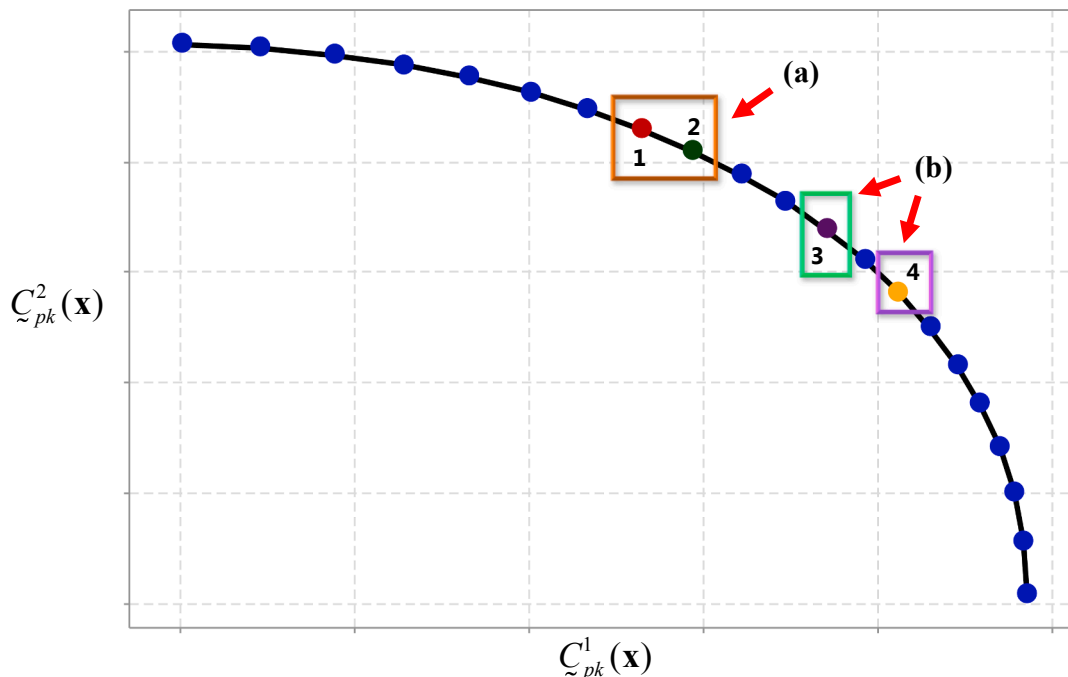


Fig. 6. Pareto frontier and confidence intervals tolerances of selected points. For a given level of risk: (a) solutions 1 and 2 are in the same confidence region. (b) solutions 3 and 4 are in different confidence regions.

**Table 3**

Control parameters and levels.

Source: Adapted from Campos [61] – co-author.

Coded Level	Control Parameters		
	Cutting speed	Feed rate	Depth of cut
	$V_c$ [m/min.]	$f$ [mm/rev.]	$a_p$ [mm]
1.682	267.62	0.26	0.39
1.000	225.00	0.22	0.33
0.000	162.50	0.16	0.24
–1.000	100.00	0.10	0.15
–1.682	57.38	0.06	0.09

using a case study for the hard turning manufacturing process without cutting fluids of AISI H13 steel with wiper ceramic tool.

### 6.1. Process background

With the increasing competition between companies, there is an increasing demand for new industrial technologies that guarantee higher levels of quality and productivity. Regarding the concerns about global warming and pollution, sustainability has attracted attention in recent decades [46]. With this, the industries have looked for better ways to perform machining of materials, such as to avoid the use of cutting fluids [47,48], using inserts with more efficient geometries [49,50] and using mathematical and statistical techniques to optimize their processes [51,52].

The turning process of hardened materials (materials in the hardness range of 45–65 HRC) has been studied for more than three decades [53]. However, many of its technologies still require further research to ensure greater generalizations, as is the case of inserts with wiper geometry. A few years ago, grinding processes were the most appropriate manufacturing strategy for the machining of hardened materials [54,55]. However, with the improvement of materials used in cutting tools and the development of new geometries, the turning operation of hardened steels is becoming common.

The tool life ( $T$ ) and surface roughness ( $Ra$ ) are response variables commonly used to characterize, respectively, productivity (CTP) and quality (CTQ) measures of hard turning processes. In the study of  $T$  and  $Ra$ , there are several influencing factors, such as cutting speed, feed rate, depth of cut and cutting tool geometry [56,57]. The use of planned experiments has become popular to study the influence of these factors, where, in the past, only the “One-factor-at-a-time” strategy was employed [58]. The analytical advantage of DOE is that we can obtain more information about the process, such as the interactions between

the factors. Among the operational advantages are fewer tests, less consumption of material and tools, and fewer machine-hours, which in general leads to lower experimentation costs [59,60].

### 6.2. Experimental procedure

For the collection of experimental data, a CCD with 8 factorial points, 6 axial points, and 5 center points was used, totaling 19 experiments based on different combinations of the levels of the control variables shown in Table 3. The experiments were performed using a CNC lathe “Kingsbury MHP 50” with 18 kW spindle power, a maximum spindle speed of 4500 rpm, tool holder tower with 12 positions, and 200 mm plate diameter. The plate has a hydraulic drive with a maximum pressure of 23 kgf/cm<sup>2</sup>, external tool holder section 20 × 20 mm and GE Fanuc numerical control, and a counterpoint with 70 mm diameter also activated by hydraulic action. The lengths in the X and Z axis are respectively 200 mm and 550 mm.

Wiper ceramic-based inserts, CC650WG, ISO code CNGA120408 T01020WG, were used. The CC650 grade used is a mixed alumina-based ceramic with chemical composition of 70% Al<sub>2</sub>O<sub>3</sub> + Ti [22.5% C, 7.5% N]. The workpieces used in the turning process were made of AISI H13 steel with chemical composition of 0.40% C, 0.35% Mn, 1.0% Si, 5.25% Cr, 1.00% V, and 1.50% Mo, dimensions Ø 50 mm × 100 mm, and an average hardness of 54 ± 1 HRC. Tool holder with negative geometry and entering angle  $\chi_r = 95^\circ$ , ISO code DCLNL 2020K12, was used to carry out the experiments. Fig. 7 shows the hard turning process with wiper CC650 tool.

For the measurement of surface roughness ( $Ra$ ), a Hommel Tester T1000 profilometer was employed in accordance with ISO/DIS 4287/1E. The tool life ( $T$ ), measured in minutes, was obtained by multiplying the total number of steps by the cutting time ( $T_c$ ) until the tool flank wear reaches the maximum allowed by the standard ISO 3685 ( $VB = 0.30$  mm), according to Eqs. (54) and (55). The wear measurement was performed after each step by using a microscope with 30 × magnification and 1- $\mu$ m resolution. Fig. 8 shows the flank and crater wear of wiper CC650 insert with  $VB = 0.30$  mm. The experimental matrix with the collected responses is presented in Table 4.

$$T_c = \frac{l_f \cdot \pi \cdot d}{1000 \cdot f \cdot V_c} \quad (54)$$

$$T = n_s T_c = \frac{n_s \cdot l_f \cdot \pi \cdot d}{1000 \cdot f \cdot V_c} \quad (55)$$

where  $l_f$  = workpiece length,  $d$  = workpiece diameter,  $n_s$  = number of steps,  $f$  = feed rate [mm/rev],  $V_c$  = cutting speed [m/min].

### 6.3. Influential parameters on response variables and the surface modelling

After the data collection, we analyzed the influences of the main effects and the interactions of the cutting parameters on the response variables. Then, response surface models were estimated using the OLS method [4,7]. This section presents the results of the modelling of the responses  $T$  and  $Ra$ , as a function of process control parameters  $V_c$ ,  $f$  and  $a_p$ . Using the data collected at factorial and center points (Table 4), analyses of the main effects and influential interactions on the response variables were performed, as shown in Fig. 9.

For the response  $T$ , the parameter  $V_c$  was the most influential, because the greater the cutting speed, the greater the wear progression in the tool, which reduces its life. The parameter  $f$  contributes to the wear progression in smaller proportions, also presenting some interaction with  $V_c$ . For the response  $Ra$ , the parameter  $f$  was the most influential, since intermediate feed rates facilitate the cutting and improve the surface quality of the machined parts. The parameters  $V_c$  and  $a_p$  also tended to provide better surface roughness when setting at intermediate levels.

By adding the axial points to the design, we applied the OLS method

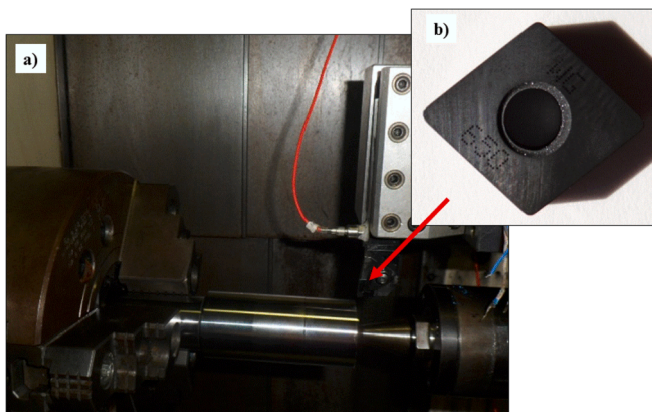


Fig. 7. Hard turning process with wiper CC650 tool. (a) Hard turning process. (b) Wiper CC650 tool.

Source: Adapted from Campos [61] – co-author.

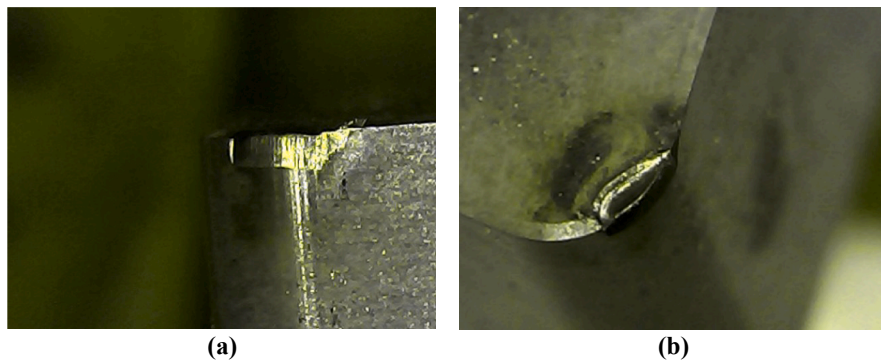


Fig. 8. Optical images of wear mechanisms. (a) Flank wear. (b) Crater wear. Source: Adapted from Campos [61] – co-author.

Table 4  
Design matrix and collected responses.  
Source: Adapted from Campos [61] – co-author.

Exp. No.	Control Parameters						Responses	
	$V_c$ [m/min.]		$f$ [mm/rev.]		$a_p$ [mm]		CTP	CTQ
	Coded	Uncoded	Coded	Uncoded	Coded	Uncoded	Maximize	Minimize
							$T$ [min.]	$Ra$ [ $\mu$ m]
1	-1.000	100.000	-1.000	0.100	-1.000	0.150	61.000	0.450
2	1.000	225.000	-1.000	0.100	-1.000	0.150	32.250	0.540
3	-1.000	100.000	1.000	0.225	-1.000	0.150	50.500	0.980
4	1.000	225.000	1.000	0.225	-1.000	0.150	30.000	1.220
5	-1.000	100.000	-1.000	0.100	1.000	0.330	62.250	0.550
6	1.000	225.000	-1.000	0.100	1.000	0.330	28.500	0.620
7	-1.000	100.000	1.000	0.225	1.000	0.330	50.500	0.930
8	1.000	225.000	1.000	0.225	1.000	0.330	27.500	0.890
9	-1.682	57.388	0.000	0.163	0.000	0.240	58.000	0.670
10	1.682	267.612	0.000	0.163	0.000	0.240	23.500	1.160
11	0.000	162.500	-1.682	0.057	0.000	0.240	37.500	0.310
12	0.000	162.500	1.682	0.268	0.000	0.240	40.000	1.250
13	0.000	162.500	0.000	0.163	-1.682	0.089	49.500	0.910
14	0.000	162.500	0.000	0.163	1.682	0.391	46.000	0.720
15	0.000	162.500	0.000	0.163	0.000	0.240	42.000	0.310
16	0.000	162.500	0.000	0.163	0.000	0.240	42.500	0.320
17	0.000	162.500	0.000	0.163	0.000	0.240	41.500	0.350
18	0.000	162.500	0.000	0.163	0.000	0.240	42.000	0.320
19	0.000	162.500	0.000	0.163	0.000	0.240	43.000	0.340

to the experimental data according to Eq. (4) to estimate the regression coefficients shown in Table 5. Then, for each response variable, we placed the regression coefficients in Eq. (1) to obtain the response surface models. Eqs. (56) and (57) provide the full quadratic models for  $T$  and  $Ra$ , respectively.

With the analysis shown in Table 5, we can see that, statistically, the tool life  $T$  of the wiper insert CC650 only depends on the linear effect of the cutting speed ( $V_c$ ) and the quadratic effect of depth of cut ( $ap^2$ ), while the surface roughness  $Ra$  of the machined parts with wiper insert CC560 depends on the linear effects of the cutting speed ( $V_c$ ) and feed rate ( $f$ ) and on the quadratic effects of the parameters  $V_c$ ,  $f$  and  $ap$ . Table 4 also reveals that the canonical models in Eqs. (56) and (57) present good fitting because they have  $R^2$  and adj.  $R^2$  close to 100%. For  $T$ , the best model was obtained, with adj.  $R^2$  equal to 92.49%.

For a better understanding of the behavior of each model, we evaluated Eqs. (56) and (57) in a graphical mesh with 225 points using

the 3D surface plot of Minitab software. Figs. 10 and 11 provide the results, showing the response surfaces as a function of the pairs of the parameters. As can be seen in the figures, the surface of  $T$  is a saddle, which implies that it has local maxima, but not a global maximum, while the surface of  $Ra$  is convex, which implies that it has a global minimum. The mathematical results of the convexity analyses are discussed in section 6.5.

#### 6.4. Sensitivity analysis

Based on the response surface models presented in Table 5, a sensitivity analysis of the cutting parameters was performed. For this, the partial derivatives of each model with respect to each design variable were obtained algebraically [62,63]. For  $T$ , we obtain:

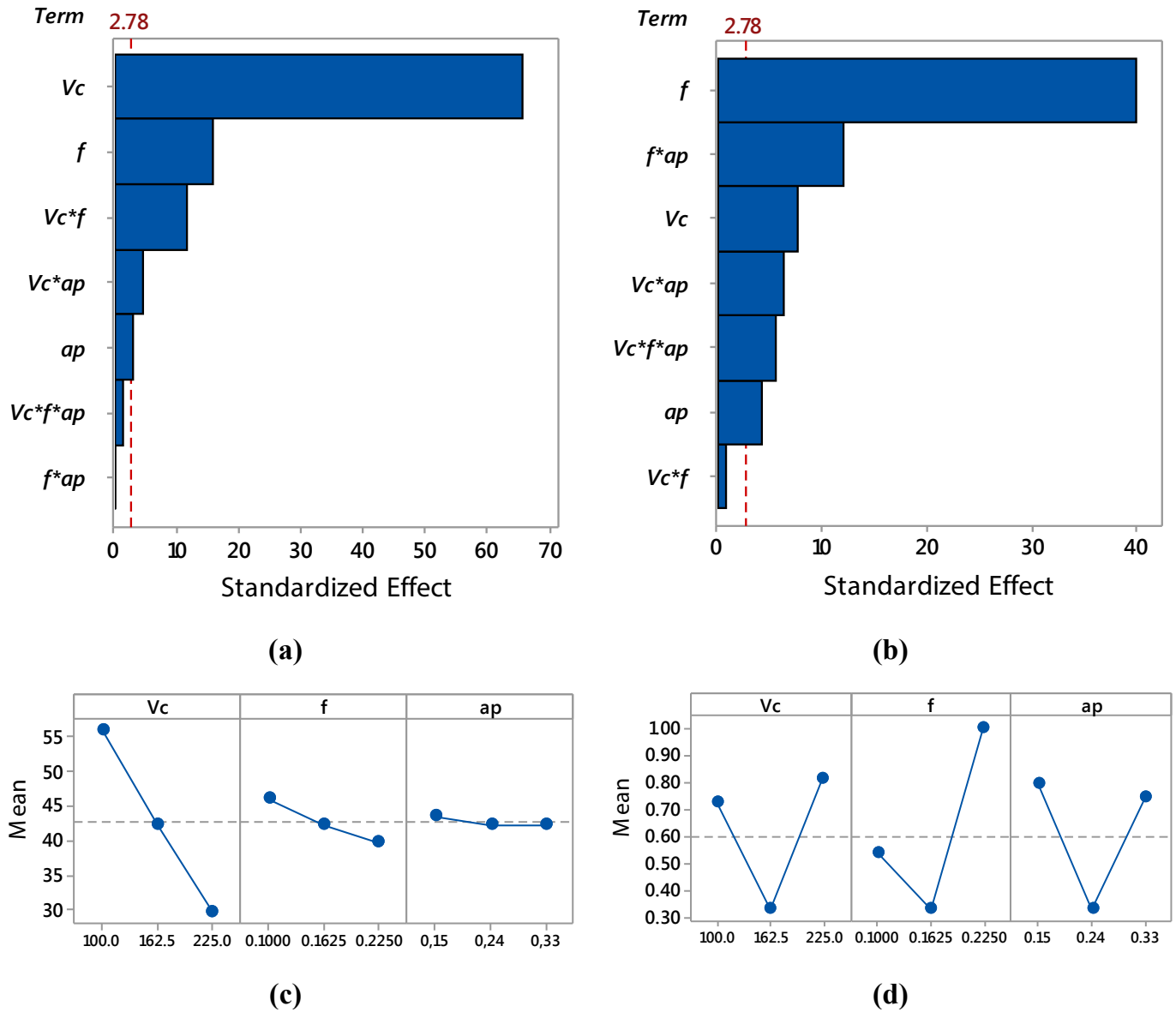


Fig. 9. Effect plots for response variables. (a) Pareto chart for  $T$ . (b) Pareto chart for  $Ra$ . (c) Main effect plot for  $T$ . (d) Main effect plot for  $Ra$ .

$$T = 42.19 - 12.01V_c - 1.56f - 0.80ap - 0.43V_c^2 - 1.14f^2 + 2.04ap^2 + 2.38V_c \times f - 0.94V_c \times ap \quad (56)$$

$$Ra = 0.33 - 0.09V_c - 0.25f - 0.04ap - 0.19V_c^2 - 0.14f^2 + 0.15ap^2 + 0.01V_c \times f - 0.04V_c \times ap - 0.07f \times ap \quad (57)$$

$$\frac{\partial T}{\partial V_c} = -12.0 - 0.86V_c + 2.38f - 0.94ap \quad (58)$$

$$\frac{\partial Ra}{\partial a_p} = -0.04 + 0.30ap - 0.08V_c - 0.07f \quad (63)$$

$$\frac{\partial T}{\partial f} = -1.56 - 2.28f + 2.38V_c \quad (59)$$

$$\frac{\partial T}{\partial a_p} = -0.80 + 4.08ap - 1.88V_c \quad (60)$$

For  $Ra$ , we obtain:

$$\frac{\partial Ra}{\partial V_c} = 0.09 + 0.38V_c + 0.01f - 0.04ap \quad (61)$$

$$\frac{\partial Ra}{\partial f} = 0.25 + 0.28f + 0.01V_c - 0.07ap \quad (62)$$

By placing the values of the planned factorial points (Table 4) in the sets of Eqs. (58)–(60) and (61)–(63), the sensitivity analysis was obtained, as shown in Fig. 12. The changes in the response variable  $T$  range from  $-16.19$  to  $+5.16$  min, which implies a variation of  $21.35$  min. The maximum alteration of  $-16.19$  min is observed when combining the high levels of the parameters  $V_c$  and  $ap$  with the low level of the parameter  $f$ , because this is a condition of greater insert wear progression. The changes in the response variable  $Ra$  range from  $-0.49$  to  $+0.61$   $\mu\text{m}$ , which implies a variation of  $1.10$   $\mu\text{m}$ . The maximum variation of  $+0.61$  is observed when combining the high levels of the parameters  $V_c$  and  $f$  with the low level of the parameter  $ap$ , because in this condition there is an increase in the material removal rate (MRR) and, therefore, in the cutting energy, contributing to higher surface

**Table 5**  
Estimated response surface models for *T* and *Ra* (in coded units).

Term	<i>T</i>					<i>Ra</i>				
	Coef	SE Coef	T-Value	P-Value	VIF	Coef	SE Coef	T-Value	P-Value	VIF
Constant	42.19	1.36	30.91	<b>0.00</b>		0.33	0.04	7.75	<b>0.00</b>	
<i>Vc</i>	-12.01	0.83	-14.53	<b>0.00</b>	1.00	0.09	0.03	3.35	<b>0.01</b>	1.00
<i>f</i>	-1.56	0.83	-1.89	0.09	1.00	0.25	0.03	9.72	<b>0.00</b>	1.00
<i>ap</i>	-0.80	0.83	-0.96	0.36	1.00	-0.04	0.03	-1.47	0.18	1.00
<i>Vc</i> * <i>Vc</i>	-0.43	0.83	-0.52	0.62	1.04	0.19	0.03	7.23	<b>0.00</b>	1.04
<i>f</i> * <i>f</i>	-1.14	0.83	-1.38	0.20	1.04	0.14	0.03	5.38	<b>0.00</b>	1.04
<i>ap</i> * <i>ap</i>	2.04	0.83	2.47	<b>0.04</b>	1.04	0.15	0.03	5.86	<b>0.00</b>	1.04
<i>Vc</i> * <i>f</i>	2.38	1.08	2.20	0.06	1.00	0.01	0.03	0.15	0.89	1.00
<i>Vc</i> * <i>ap</i>	-0.94	1.08	-0.87	0.41	1.00	-0.04	0.03	-1.11	0.30	1.00
<i>f</i> * <i>ap</i>	0.00	1.08	0.00	1.00	1.00	-0.07	0.03	-2.07	0.07	1.00
R-sq (%)	96.25					95.76				
Adj. R-sq (%)	92.49					91.53				

Note: Significant terms (p-value < 5%) are highlighted in bold.

roughness [64,65].

These changes can also be taken in percentage terms. If we assume the difference between the highest and the lowest observations of Table 4 as the maximum range for each response variable in the design space considered, then we can use this information to normalize the sensitivity analysis of Fig. 12. Thus, we can infer about the behavior of both responses in standardized units (or, in percentage terms). In Table 4, the highest and lowest values of *T* are respectively 62.25 min and 23.50 min, which provides a range of 38.75 min. For *Ra*, the highest and lowest values are, respectively, 1.25 and 0.31 μm, which

provides a range of 0.94 μm. By dividing the previously mentioned extreme values by the ranges of each response, we obtain that, for *T*, there is a percentage change from -49.03% (-16.19/38.75) to +13.32% (+5.16/38.75) and, for *Ra*, there is a percentage change from -52.13% (-0.49/0.94) to +64.89% (+0.61/0.94) μm. These results allow us to conclude that in the design space considered, *Ra* is more sensitive to changes in control parameters, thus a more difficult response to control.

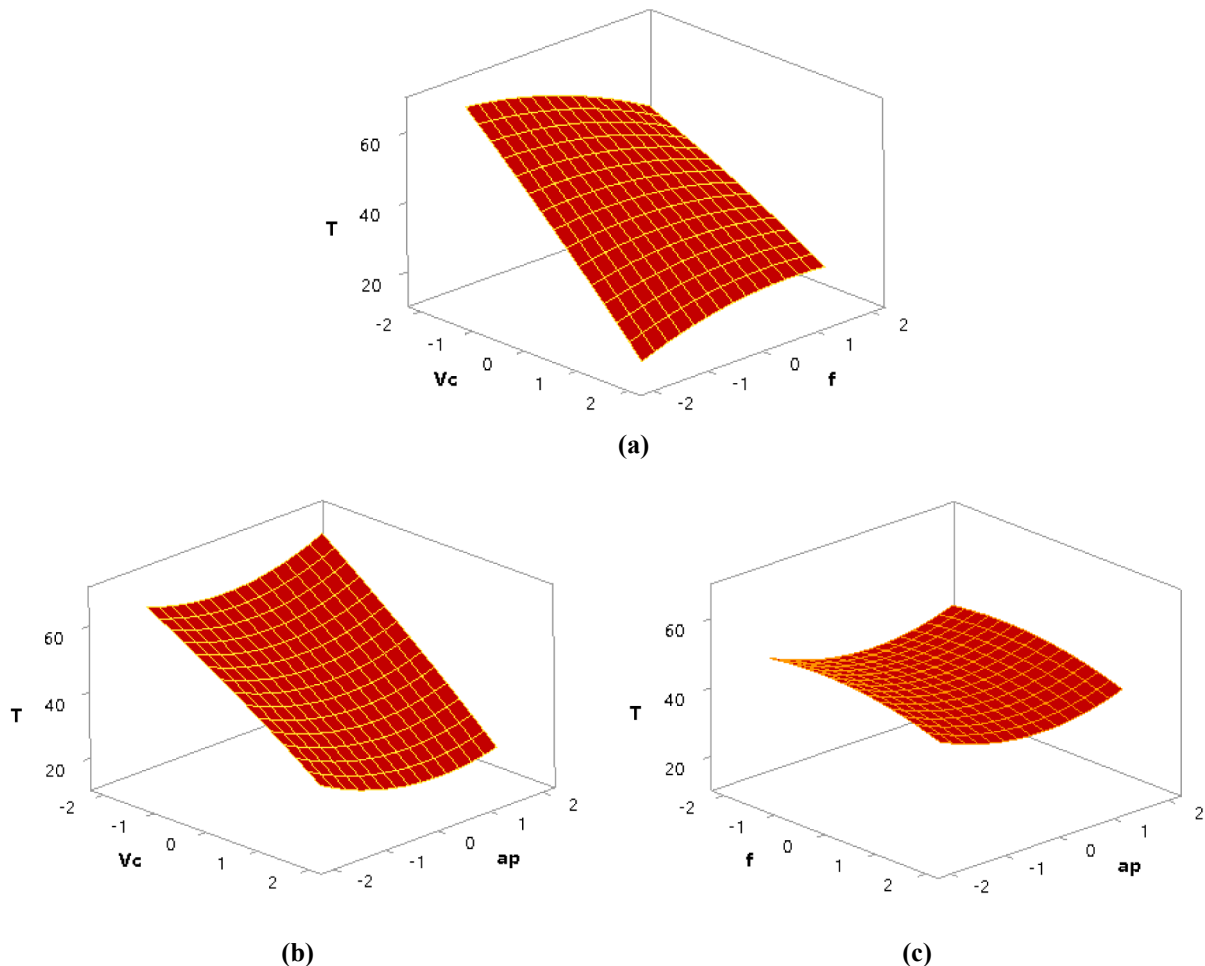


Fig. 10. Response surface for *T*: (a) *Vc* vs *f*, *ap*=0. (b) *Vc* vs *ap*, *f*=0. (c) *f* vs *ap*, *Vc*=0.

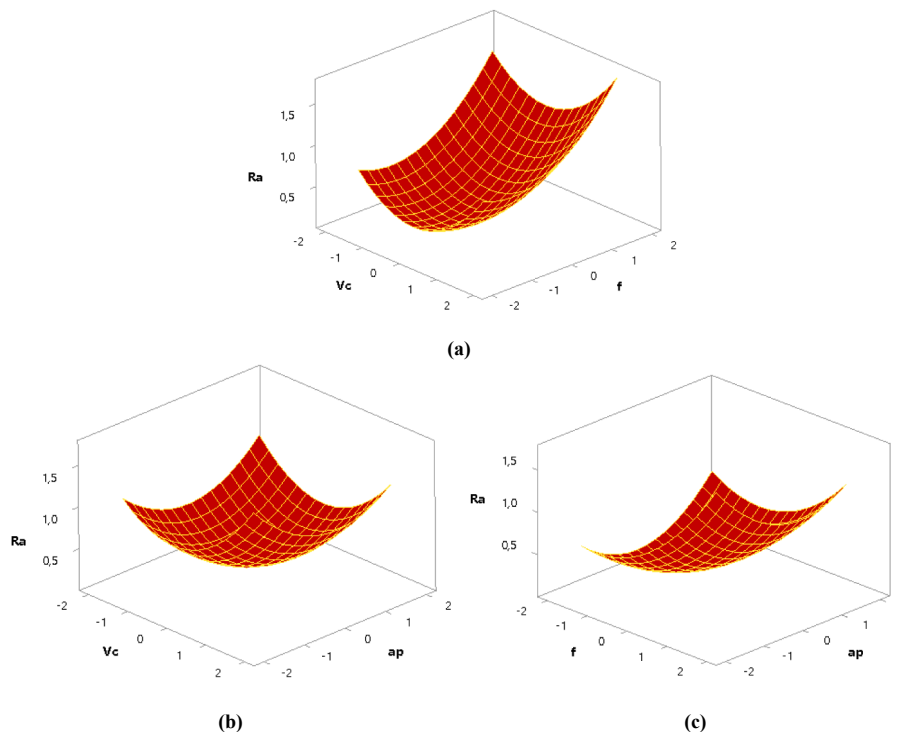


Fig. 11. Response surface for Ra: (a)  $V_c$  vs  $f$ ,  $ap=0$ . (b)  $V_c$  vs  $ap$ ,  $f=0$ . (c)  $f$  vs  $ap$ ,  $V_c=0$ .

6.5. Traditional approach: Bi-objective optimization of original variables

Once the response surface models are known, process optimization can be performed using the models as objective functions of the optimization problem. Prior to this step, some caution is required, such as convexity analysis. For  $T$ , the model has both positive and negative eigenvalues [2.1461; -2.0431; 0.3716], which denotes a saddle function. For  $R_a$ , the model has only positive eigenvalues [0.2012; 0.1687; 0.1088], which denotes a convex function.

Considering the nature of the process investigated, it is desired to obtain the maximum tool life  $T$  and the minimum surface roughness  $R_a$  for the parts. Since the model for  $T$  is a saddle, the stationary point will not be the individual optimum because the maximization direction will

lead to a local maximum usually located at the boundary of the experimental design. This demonstrates that the use of the experimental spherical region constraint is mandatory for the optimization of  $T$  [66]. On the other hand, since the model for  $R_a$  is convex, the stationary point will be the individual optimal since there is a minimization direction. The convexity analysis also indicates that the WS method is not appropriate to optimize  $T$  and  $R_a$  concomitantly, because the multi-objective problem has functions with different convexities [35]. These results motivated the use of NBI restricted to the experimental region constraint in this work.

Using the traditional NBI method introduced in Eq. (49), the functions of interest are first scaled by a pay-off matrix  $\Phi$ , obtained from the individual optimizations of  $f_1(x)$  and  $f_2(x)$ , subjected to the

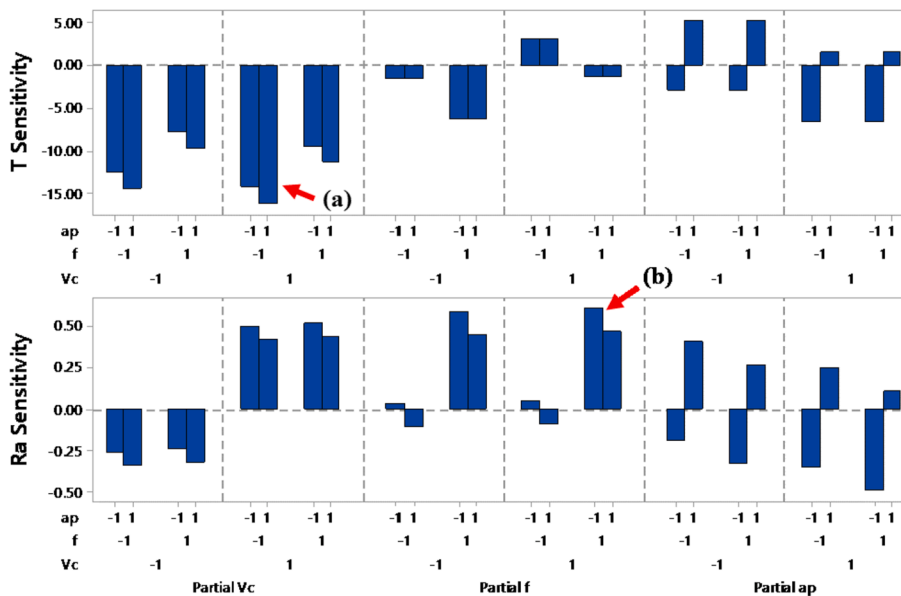


Fig. 12. Sensitivity analysis for  $T$  and  $R_a$ . (a) Extreme alteration of  $T$ . (b) Extreme alteration of  $R_a$ .

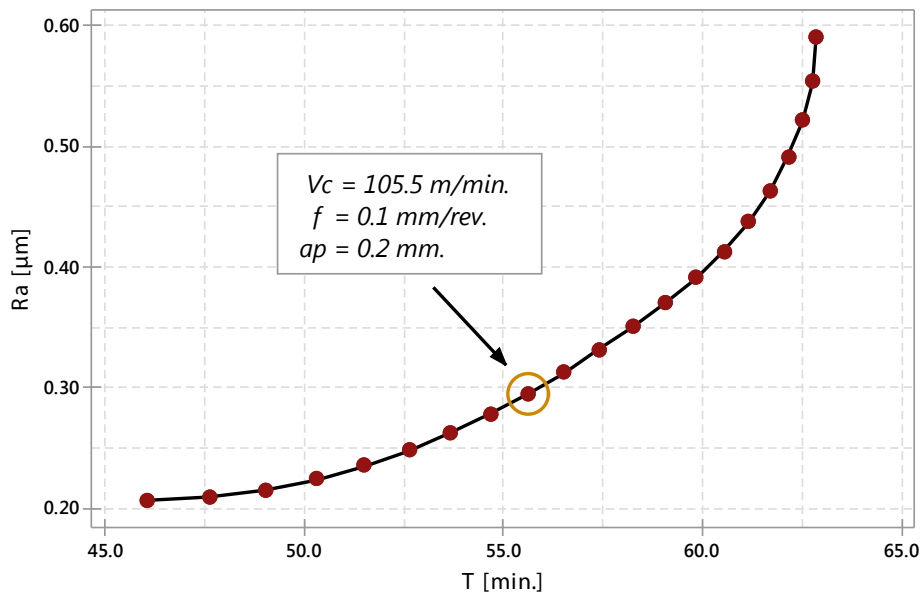


Fig. 13. Pareto frontier for  $T$  and  $Ra$ .

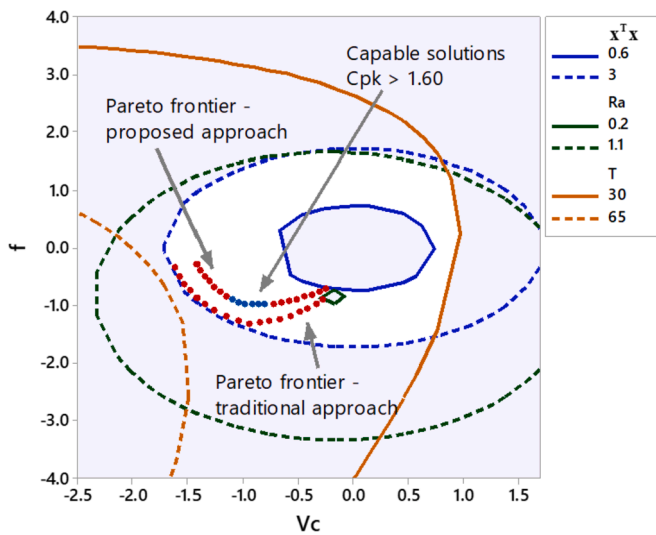


Fig. 14. Pareto frontiers inside the feasible region for traditional and proposed approaches.

experimental region constraint, such that  $g_j(x) = \mathbf{x}^T \mathbf{x} - \rho^2 \leq 0$  or  $g_j(x) = \mathbf{x}^T \mathbf{x} \leq \rho^2$ . This constraint guarantees that the optimal solutions will lie within the design space. For solving the individual optimizations, we employed the Generalized Reduced Gradient (GRG) algorithm. The numerical results are shown in Eq. (64):

$$\Phi = \begin{pmatrix} f_1^U & f_1^N \\ f_2^N & f_2^U \end{pmatrix} = \begin{pmatrix} 62.845 & 46.006 \\ 0.590 & 0.207 \end{pmatrix} \quad (64)$$

where  $N$  and  $U$  indicate the nadir and utopia solutions, respectively.

Then, by applying Eq. (37), we obtain the scaled function as follows:

$$\bar{f}_1(\mathbf{x}) = \left[ \frac{f_1(\mathbf{x}) - f_1^U}{f_1^N - f_1^U} \right] = \left[ \frac{f_1(\mathbf{x}) - 62.845}{-16.839} \right] \quad (65)$$

$$\bar{f}_2(\mathbf{x}) = \left[ \frac{f_2(\mathbf{x}) - f_2^U}{f_2^N - f_2^U} \right] = \left[ \frac{f_2(\mathbf{x}) - 0.207}{0.383} \right] \quad (66)$$

With the application of the GRG algorithm as a subroutine of the bi-objective problem via NBI formulated in Eq. (49), the optimal

combinations of  $T$  and  $Ra$  are obtained as a function of the cutting parameters  $V_c$ ,  $f$  and  $a_p$ . Fig. 13 shows the resulting Pareto frontier, containing 21 solutions to the problem. Fig. 14 shows the Pareto frontier for the traditional approach within the feasible region formed by the overlaid contour plots of the responses and the right-hand side of the experimental region constraint  $g_j(x) = \mathbf{x}^T \mathbf{x} \leq \rho^2$ .

As can be seen in Figs. 13 and 14, the responses are of a conflicting nature, since an increase in  $T$  (a desirable outcome) leads to an increase in  $Ra$  (an undesirable outcome) and a decrease in  $Ra$  (a desirable outcome) leads to a decrease in  $T$  (an undesirable outcome). Despite this conflict, a Pearson correlation analysis demonstrated that these responses are linearly independent ( $\rho_{T|Ra} = -0.252$ ;  $p$ -value = 0.299).

In this work, we demonstrate that the decision maker should opt for combinations that best favor the reality of the process investigated. To illustrate this decision making, solution 9 was highlighted in Figs. 13 and 14, showing that a tool life  $T$  of approximately 55.6 min and a surface roughness  $Ra$  of approximately 0.255  $\mu\text{m}$  can be obtained simultaneously with the optimum set up  $V_c = 105.5 \text{ m/min}$ ,  $f = 0.1 \text{ mm/rev}$ . and  $a_p = 0.2 \text{ mm}$ . This surface roughness is suitable for finishing operations and is usually obtained with grinding processes [67,68]. If the experimenter is interested in using the hard turning process without cutting fluid as an alternative to the grinding process, solution 9 provides a good result for  $Ra$  (the CTP characteristic) while allowing the extension of  $T$  (the CTP characteristic). The set of optimal combinations obtained in this study is presented in Table 6. As can be seen in the table, no solution presents satisfactory capability ratios for both responses considering the acceptable value for critical parameters/new process with one-sided specification limit ( $C_{pk} \geq 1.60$ ) and that solution 9 is one of the solutions with the best global result ( $C_{pk} \cong 1.50$ ).

Table 7 shows confidence intervals for  $T$  and  $Ra$  in optimal solution 9 calculated by Eq. (18), showing that the confidence interval for  $T$  is narrower than the confidence interval for  $Ra$ . Figs. 15 and 16 present a process simulation for the experimentally observed response benchmarks (Table 4) and the optimal solution 9. Table 4 shows that, for  $T$ , experiment 5 provides the best mean value ( $T = 62.50 \text{ min}$ ), and, for  $Ra$ , both experiments 11 and 15 provide the best mean value ( $Ra = 0.310 \mu\text{m}$ ); however, experiment 15 provides a better value for  $T$  ( $T = 42.00 \text{ min}$ ), which makes it a more appropriate benchmark. Based on Figs. 15 and 16, we demonstrate that the optimization procedure can find suitable mean solutions between (Fig. 15) or even better than the benchmarks (Fig. 16). However, due to the variability effect, their probability distributions may not differentiate much, producing quality

**Table 6**  
Optimal solutions for the process investigated.

No.	$w_i$	Coded control parameters			Responses			
					Optimized		Calculated	
		$V_c$ [m/min.]	$f$ [mm/rev.]	$ap$ [mm]	$T$ [min.]	$Ra$ [ $\mu$ m]	$C_{pk}(T)$	$C_{pk}(Ra)$
1	0.000	-0.231	-0.928	-0.117	46.0060	0.2070	0.0000	2.9086
2	0.050	-0.343	-0.935	-0.142	47.5868	0.2093	0.3649	2.8018
3	0.100	-0.444	-0.946	-0.167	49.0017	0.2155	0.6643	2.6480
4	0.150	-0.536	-0.960	-0.190	50.2925	0.2244	0.9063	2.4647
5	0.200	-0.620	-0.976	-0.214	51.4865	0.2355	1.0990	2.2662
6	0.250	-0.700	-0.993	-0.236	52.6022	0.2484	1.2493	2.0624
7	0.300	-0.774	-1.011	-0.258	53.6532	0.2628	1.3650	1.8618
8	0.350	-0.845	-1.030	-0.279	54.6495	0.2785	1.4517	1.6680
9	0.400	-0.912	-1.050	-0.301	55.5989	0.2952	1.5153	1.4847
10	0.450	-0.976	-1.070	-0.321	56.5076	0.3128	1.5608	1.3134
11	0.500	-1.036	-1.091	-0.342	57.3805	0.3312	1.5907	1.1536
12	0.550	-1.095	-1.112	-0.364	58.2216	0.3504	1.6092	1.0062
13	0.600	-1.151	-1.133	-0.384	59.0343	0.3702	1.6197	0.8710
14	0.650	-1.215	-1.104	-0.367	59.8114	0.3908	1.6763	0.7708
15	0.700	-1.282	-1.040	-0.320	60.5155	0.4131	1.7601	0.6839
16	0.750	-1.346	-0.974	-0.262	61.1413	0.4371	1.8383	0.5915
17	0.800	-1.405	-0.904	-0.192	61.6856	0.4630	1.9123	0.4932
18	0.850	-1.460	-0.828	-0.112	62.1430	0.4909	1.9849	0.3880
19	0.900	-1.508	-0.745	-0.018	62.5036	0.5210	2.0578	0.2738
20	0.950	-1.549	-0.650	0.084	62.7494	0.5537	2.1351	0.1469
21	1.000	-1.582	-0.536	0.193	62.8449	0.5898	2.2184	0.0000

**Table 7**  
Confidence intervals for  $T$  and  $Ra$  in optimal solution 9.

Response	Lower Limit	Mean	Upper Limit
$T$	51.5224	55.5989	59.9679
$Ra$	0.1688	0.2952	0.4335

( $Ra$ ) or performance ( $T$ ) losses. Moreover, the probability distribution of  $T$  differs more from the distributions of the benchmarks than the distribution of the optimum of  $Ra$ . This demonstrates that  $Ra$  is a response variable that is more difficult to control because it presents greater variability, as was also explained in the sensitivity analysis of section 6.4. Similar results were found by Rocha et al. [45] for the hard turning of AISI H13 steel with wiper 6050 tool.

To deal with the effects of variability on the responses studied, we apply the proposed optimization strategy based on capability ratios in the following section.

6.6. Proposed approach: bi-objective optimization of capability ratios

In this section, we present the application of the proposed approach for the hard turning process investigated. Since we desire the maximum  $T$  and the minimum  $Ra$ , we can obtain the ratios  $C_{pk}(x)$  for  $T$  and  $Ra$  by applying Eqs. (33) and (34).

For  $T$ , we have:

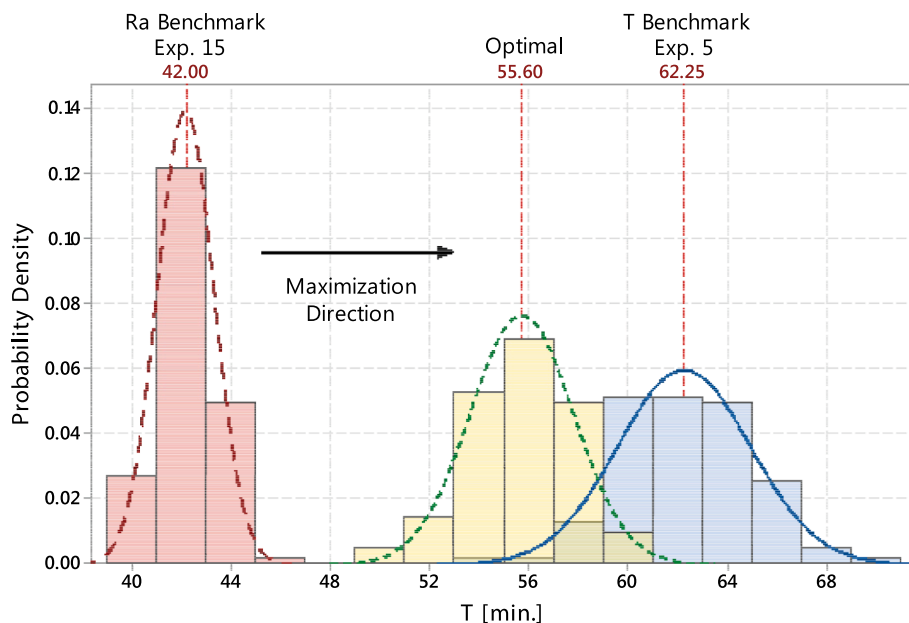


Fig. 15. Process simulation for  $T$  considering  $Ra$  and  $T$  benchmarks and a convenient mean optimal solution.

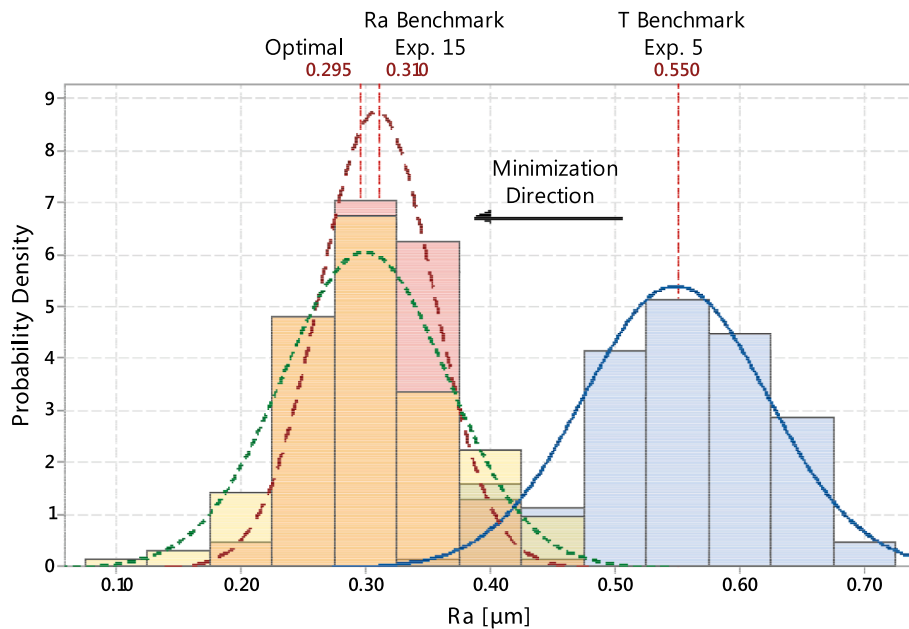


Fig. 16. Process simulation for Ra considering Ra and T benchmarks and a convenient mean optimal solution.

$$\begin{aligned}
 C_{pk}^1(\mathbf{x}) &= \frac{E[Y_1(\mathbf{x})] - LSL}{3 \cdot \sqrt{\text{Var}[Y_1(\mathbf{x})|x_0]}} \\
 &= \frac{[f_1(\mathbf{x}) - f_1^N]}{3 \cdot \sigma_{f_1(\mathbf{x})} \sqrt{[x_0^{(m)T} (\mathbf{X}^T \mathbf{X})^{-1} x_0^{(m)}]}} \\
 &= \frac{[f_1(\mathbf{x}) - 46.006]}{3 \cdot (3.055) \sqrt{[x_0^{(m)T} (\mathbf{X}^T \mathbf{X})^{-1} x_0^{(m)}]}}
 \end{aligned}$$

(67)

$$\begin{aligned}
 C_{pk}^2(\mathbf{x}) &= \frac{USL - E[Y_2(\mathbf{x})]}{3 \cdot \sqrt{\text{Var}[Y_2(\mathbf{x})|x_0]}} \\
 &= \frac{[f_2^N - f_2(\mathbf{x})]}{3 \cdot \sigma_{f_2(\mathbf{x})} \sqrt{[x_0^{(m)T} (\mathbf{X}^T \mathbf{X})^{-1} x_0^{(m)}]}} \\
 &= \frac{[0.590 - f_2(\mathbf{x})]}{3 \cdot (0.096) \sqrt{[x_0^{(m)T} (\mathbf{X}^T \mathbf{X})^{-1} x_0^{(m)}]}}
 \end{aligned}$$

(68)

For Ra, we have:

By performing the individual optimizations of these functions as formulated in Eq. (35), we find the Utopia and Nadir points as shown in Eq. (69). This equation is the version of the pay-off matrix in Eq. (36) for the bi-objective case:

Table 8  
Optimal solutions for the investigated process.

No.	w	Coded control parameters			Responses			
					Optimized		Calculated	
		Vc [m/min.]	f [mm/rev.]	ap [mm]	Cpk (T)	Cpk (Ra)	T [min.]	Ra[μm]
1	0.000	-0.237	-0.756	-0.069	0.0000	3.0355	45.8535	0.2048
2	0.050	-0.303	-0.747	-0.078	0.2256	3.0182	46.7164	0.2047
3	0.100	-0.367	-0.736	-0.084	0.4371	2.9865	47.5313	0.2064
4	0.150	-0.427	-0.724	-0.090	0.6359	2.9417	48.3050	0.2096
5	0.200	-0.486	-0.712	-0.094	0.8230	2.8848	49.0431	0.2141
6	0.250	-0.543	-0.699	-0.097	0.9991	2.8167	49.7497	0.2199
7	0.300	-0.597	-0.685	-0.099	1.1648	2.7379	50.4289	0.2268
8	0.350	-0.651	-0.671	-0.099	1.3205	2.6488	51.0844	0.2348
9	0.400	-0.704	-0.657	-0.099	1.4666	2.5497	51.7210	0.2438
10	0.450	-0.756	-0.642	-0.096	1.6032	2.4410	52.3391	0.2539
11	0.500	-0.807	-0.627	-0.093	1.7305	2.3225	52.9460	0.2649
12	0.550	-0.858	-0.611	-0.086	1.8484	2.1945	53.5401	0.2770
13	0.600	-0.909	-0.595	-0.080	1.9568	2.0567	54.1308	0.2903
14	0.650	-0.961	-0.579	-0.071	2.0555	1.9089	54.7175	0.3048
15	0.700	-1.014	-0.562	-0.059	2.1443	1.7509	55.3049	0.3206
16	0.750	-1.067	-0.544	-0.044	2.2225	1.5821	55.8978	0.3381
17	0.800	-1.123	-0.526	-0.026	2.2897	1.4019	56.5005	0.3574
18	0.850	-1.180	-0.506	-0.003	2.3448	1.2092	57.1190	0.3791
19	0.900	-1.241	-0.486	0.026	2.3867	1.0030	57.7624	0.4035
20	0.950	-1.306	-0.464	0.061	2.4137	0.7815	58.4413	0.4316
21	1.000	-1.376	-0.440	0.107	2.4234	0.5421	59.1719	0.4645

Note: capable solutions for both responses are highlighted in bold.

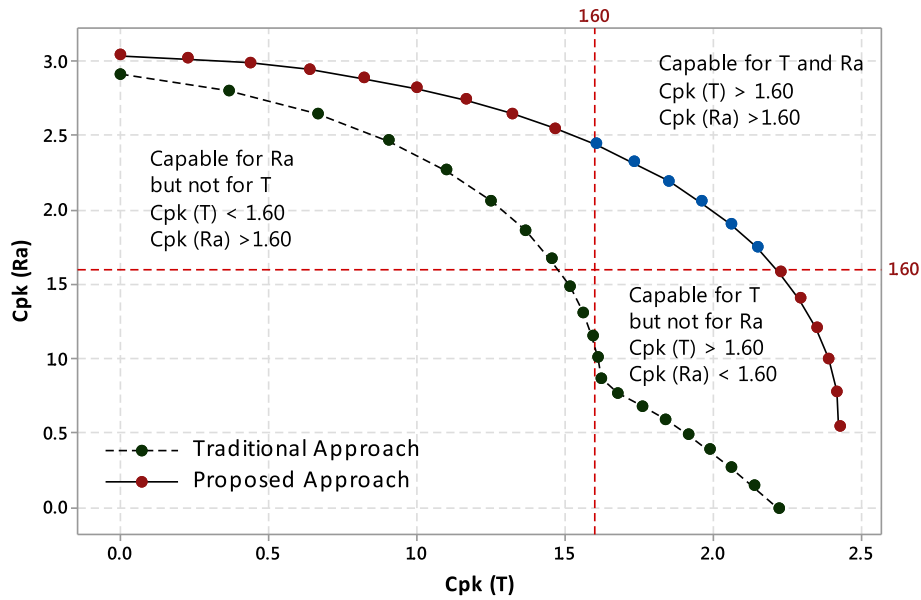


Fig. 17. Pareto frontier for Cpk (T) and Cpk (Ra) with capability clusters of optimal solutions. Note: The blue points indicate that the proposed approach can find capable solutions for both T and Ra.

$$K = \begin{pmatrix} C_{pk}^{1,U} & C_{pk}^{1,N} \\ C_{pk}^{2,N} & C_{pk}^{2,U} \end{pmatrix} = \begin{pmatrix} 2.423 & 0.000 \\ 0.542 & 3.035 \end{pmatrix} \quad (69)$$

Then, with the application of Eqs. (41) and (42), we obtain the scaled functions as follows:

$$\begin{aligned} \bar{C}_{pk}^1(\mathbf{x}) &= \left[ \frac{C_{pk}^1(\mathbf{x}) - C_{pk}^{1,U}}{C_{pk}^{1,N} - C_{pk}^{1,U}} \right] = \left[ \frac{C_{pk}^1(\mathbf{x}) - 2.423}{-2.423} \right] \\ \bar{C}_{pk}^2(\mathbf{x}) &= \left[ \frac{C_{pk}^2(\mathbf{x}) - C_{pk}^{2,U}}{C_{pk}^{2,N} - C_{pk}^{2,U}} \right] = \left[ \frac{C_{pk}^2(\mathbf{x}) - 3.035}{2.493} \right] \end{aligned} \quad (70)$$

And the optimization problem using NBI can be formulated as previously introduced in Eq. (51):

$$\begin{aligned} \text{Min} F(\mathbf{x}) &= \bar{C}_{pk}^1(\mathbf{x}) \\ \text{s. t. : } & \bar{C}_{pk}^1(\mathbf{x}) - \bar{C}_{pk}^2(\mathbf{x}) + 2w - 1 = 0 \\ & \mathbf{x} \in \Omega \\ & g_j(\mathbf{x}) = \mathbf{x}^T \mathbf{x} - p^2 \leq 0 \\ & h_{j+1}(\mathbf{x}) = 0 \end{aligned} \quad (71)$$

For different weights  $w$ , we obtain the optimal solutions presented in Table 8 by using the GRG algorithm. Fig. 17 provides the Pareto frontier for ratios  $C_{pk}(\mathbf{x})$  and Fig. 18 presents the Pareto frontier converted to the original variables. In both figures, we indicate the capability clusters. Differently from what we observed in the traditional approach of section 6.5, in this case, we obtain several solutions with acceptable capability ( $C_{pk}(\mathbf{x}) \geq 1.60$ ).

Similar results can also be found with the application of the other

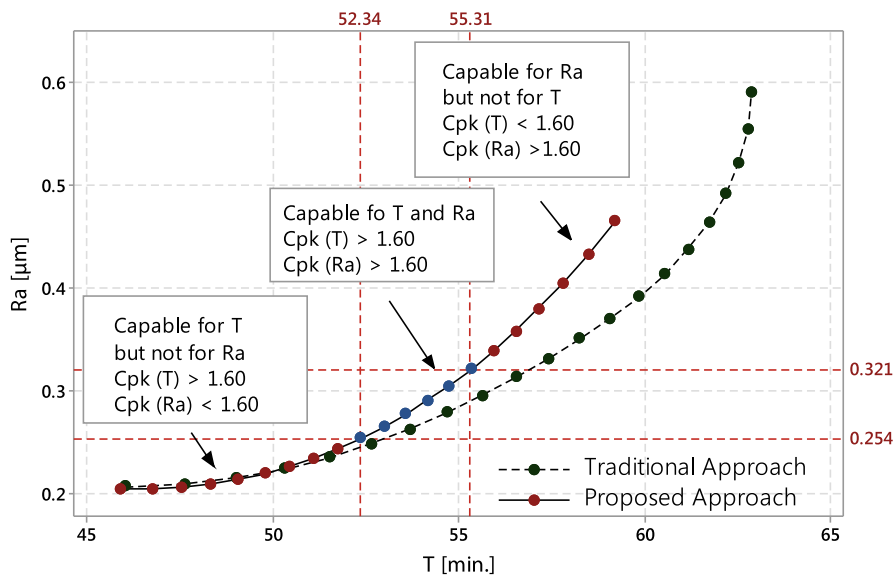


Fig. 18. Pareto frontier for original variables T and Ra with capability clusters of optimal solutions. Note: The blue points indicate that the proposed approach can find capable solutions for both responses where the traditional approach finds good mean values with unfavorable variance.

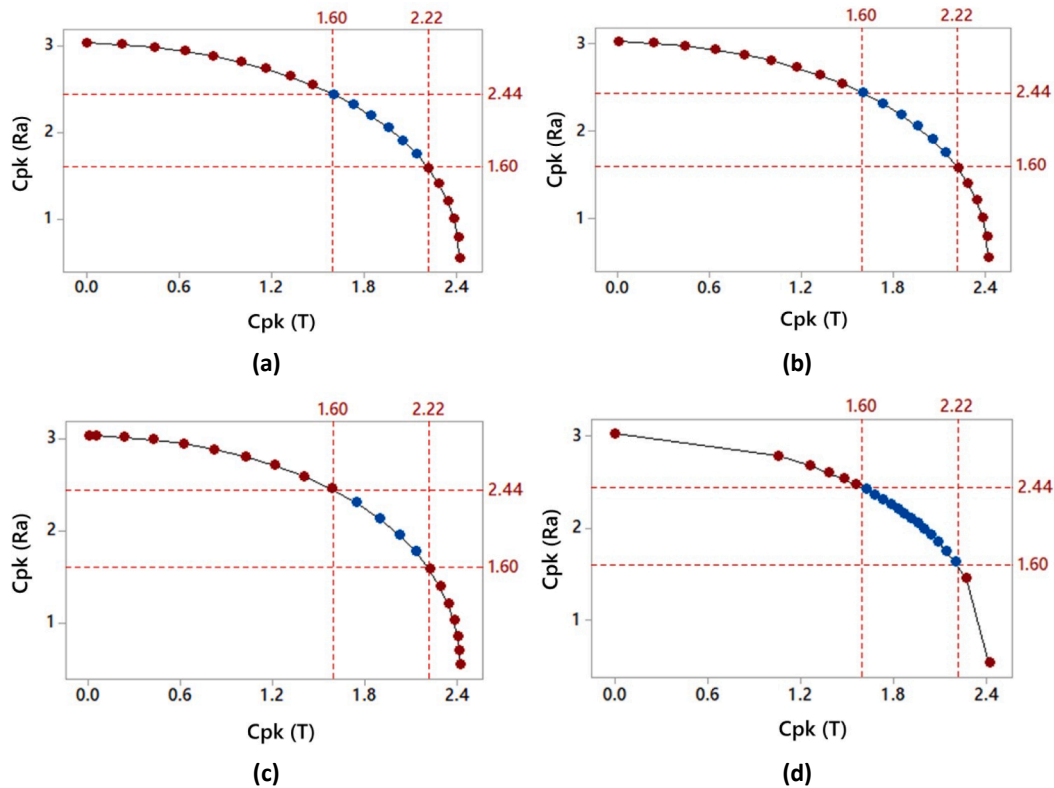


Fig. 19. Pareto frontiers for Cpk (T) and Cpk (Ra) obtained with different multiobjective methods. (a) NBI. (b) NNC. (c) WS. (d) GCM. Note: The blue points indicate capable solutions for both T and Ra.

Table 9  
Confidence intervals for T and Ra in optimal solution 14.

Response	Lower Limit	Mean	Upper Limit
T	51.8108	54.7175	58.5384
Ra	0.2176	0.3048	0.4285

numerical methods introduced in section 4. As can be seen in Fig. 19, the NBI (Fig. 19a) and NNC (Fig. 19b) methods provide identical Pareto frontiers, which was expected regarding their close mathematical fundamentals [39,40]. Furthermore, they were the only to offer evenly distributed solutions (known as one of the best advantages of them) with six capable solutions. By applying Eq. (30), the WS method concentrated some solutions close to the anchor points and provided four capable solutions (Fig. 19c). Finally, by applying Eq. (31), the GCM concentrated almost all solutions in the frontier center (Fig. 19d); although this could be seen as a satisfactory result, given the purpose of finding capable solutions for both responses, these solutions may be indistinguishable in practice because of the variability effect. This problem is discussed in the following paragraphs.

Assuming again that the experimenter is interested in using the hard turning process without cutting fluid as an alternative to the grinding process, we can select the solution 14 as an appropriate cutting condition in Table 8 because it provides a surface roughness Ra near 0.30 μm and a tool life T of about 55 min (mean values close to those obtained with solution 9 in Table 6). Table 9 displays the confidence interval for this solution according to Eq. (18). As can be seen in the table, for both response variables, the proposed approach narrowed the confidence interval, but, for T, the result was better.

As previously shown in Fig. 14, in the proposed approach, the frontier is shifted to a region closer to the design center, where the prediction variance is smaller. With this process, the mean solutions for Ra are more favored, since Ra is a convex function and presents the

minimum point closest to the design center (see the green and the blue lines in Fig. 14). On the other hand, the mean solutions of T become worse, since T is a saddle-shaped function and presents local maximum at the boundaries of the design (see the orange and the blue lines in Fig. 14).

Despite this, with the proposed strategy, the decision maker can choose to lose a little in mean values and gain in prediction capability, which can benefit production with higher precision and lower rates of non-conformities and inefficiencies. Fig. 20 presents a simulation for the solutions selected with the traditional approach (section 6.5) and with the proposed strategy. With the chosen solution, we lose more in the expected value of T, but for both responses, there is a reduction of variability, as initially proposed.

By applying Eqs. (52) and (53), we found the sample sizes for detecting differences between the Pareto optimal solutions showed in Table 8. In Table 10, we provide the sample sizes for different pairs of solutions (all composed by solution 14). For instance, to identify the difference between the capability ratios  $C_{pk}(x)$  of solutions 14 and 16, it is necessary to measure 40 samples for T ( $n_1$ ) and 9 samples for Ra ( $n_2$ ), considering a risk probability  $\beta_{risk}$  of 0.20. However, for solutions 13 and 14, with the same  $\beta_{risk}$  of 0.20, we obtain  $n_1 = 115$  and  $n_2 = 40$ , since the incremental differences  $\delta_1$  and  $\delta_2$  are smaller. In Table 10, we also provide the sample sizes for different risk probabilities  $\beta_{risk}$ , considering that the decision maker can choose the acceptable level of risk depending on the application.

If the decision maker considers that sample sizes of 141–189 are very large to detect differences between solutions 14 and 15, it will be possible to consider them as coincident solutions in practice. Moreover, this result may serve to feedback the construction of the Pareto frontier, since the 21 solutions were found with weight increments of 0.05 from  $w = 0.00$  to  $w = 1.00$ , as regularly used in the literature [14,37,44]. If adjacent solutions lie in the same confidence regions, the weight increments could be changed to 0.10; therefore providing 11 more distinguishable solutions.

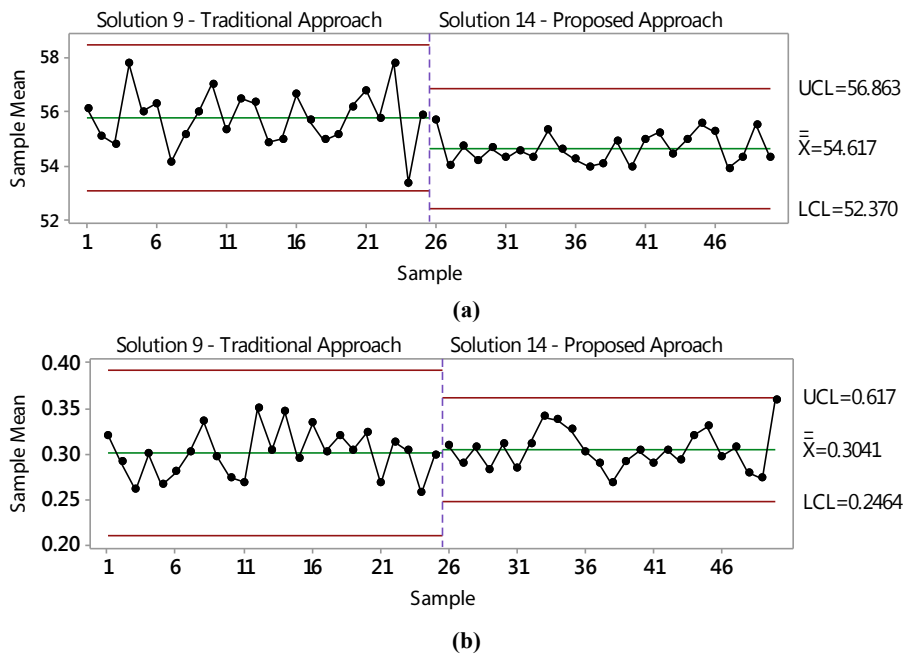


Fig. 20. Comparison between simulated results obtained with traditional and proposed approaches. (a) Simulated results for  $T$ . (b) Simulated results for  $Ra$ .

7. Conclusions

In this work, we proposed a multiobjective optimization strategy based on capability ratios. We used the prediction variance as a measure of the design capability of providing predictable optimal results. Also, we advocated that the natural limits for the original response variables were the individual nadir solutions. Then, we developed a modified capability ratio for the optimization of both the original response variables and the model variance.

To illustrate the feasibility of the proposed approach, we analyzed the turning process of AISI H13 steel with wiper CC650 tool. Planned experiments based on a CCD for the three control parameters  $V_c$ ,  $f$  and  $ap$  were employed to model the tool life  $T$  and surface roughness  $Ra$ . Since the estimated regression models presented good fitting, we formulated the optimization problems using them as objective functions.

First, to solve the traditional bi-objective problem for  $T$  and  $Ra$ , we applied the NBI-GRG method; with this procedure, we obtained different optimal combinations of process parameters and built the Pareto frontier. Based on this, we demonstrated the conflicting nature of the

responses, showing that the decision maker should choose the optimal combinations that best favor the application investigated. In addition, we showed that the traditional approach is appropriate for optimizing mean values but not for obtaining predictable optimal solutions.

Then, we applied the proposed approach to the turning process studied. For this, we employed the NBI-GRG method to obtain the solutions of the bi-objective problem for the capability ratios of  $T$  and  $Ra$ . With this procedure, we obtained evenly distributed Pareto frontiers for both the capability ratios and the original response variables. Afterward, we compared them to the previous frontier and the capability data obtained with the traditional approach. Finally, we also compared them to other numerical methods and found that the NBI and the NNC methods were the most advantageous in obtaining evenly distributed frontiers.

From this work, the following major conclusions can be drawn:

- The proposed approach was able to find a satisfactory set of optimal solutions with satisfactory prediction capabilities for both responses of interest, considering a case of turning with a reduced number of

Table 10  
Sample sizes for detecting differences between Pareto optimal solutions for  $C_{pk}(x)$ .

Solutions	$\beta_{risk}$	Power	$\delta_1$	$\delta_2$	$\sigma_1$	$\sigma_2$	$\delta_1/\sigma_1$	$\delta_2/\sigma_2$	$n_1$	$n_2$
12,14	0.10	0.90	0.207	0.138	0.376	0.333	0.551	0.413	35	62
	0.15	0.85	0.207	0.138	0.376	0.333	0.551	0.413	30	53
	0.20	0.80	0.207	0.138	0.376	0.333	0.551	0.413	26	47
13,14	0.10	0.90	0.099	0.148	0.376	0.333	0.262	0.443	154	54
	0.15	0.85	0.099	0.148	0.376	0.333	0.262	0.443	131	46
	0.20	0.80	0.099	0.148	0.376	0.333	0.262	0.443	115	40
14,15	0.10	0.90	0.089	0.158	0.376	0.333	0.236	0.474	189	47
	0.15	0.85	0.089	0.158	0.376	0.333	0.236	0.474	162	40
	0.20	0.80	0.089	0.158	0.376	0.333	0.236	0.474	141	35
14,16	0.10	0.90	0.167	0.327	0.376	0.333	0.444	0.980	54	11
	0.15	0.85	0.167	0.327	0.376	0.333	0.444	0.980	46	10
	0.20	0.80	0.167	0.327	0.376	0.333	0.444	0.980	40	9

Note: the standard deviations  $\sigma_1$  and  $\sigma_2$  are the same for all comparisons, since the solution 14 is taken as the null hypothesis.

center points, a saddle-shaped function for  $T$  and a convex function for  $Ra$ , with conflicting objectives.

- The Pareto frontier obtained with the proposed strategy was shifted to a region closer to the design center, without greatly impairing the mean values of the original responses. This was made possible by the joint optimization of mean and prediction variance via the proposed modified capability ratio.
- Although  $Ra$  is a more difficult variable to control, the proposed optimization strategy allowed it to be favored both with respect to mean values and prediction capability, which was a desired result. This occurred because  $Ra$  was modeled by a convex function, with minimization direction, and its stationary point was closer to the design center, where the prediction variance is naturally smaller.
- For non-immediately consecutive solutions, with risk probabilities greater than 0.10, sample sizes less than 62 are required to detect differences between them. Larger sample sizes are needed to identify differences between adjacent solutions.

- The identification of adjacent solutions within a single confidence region can serve as an argument to feedback optimization via NBI with larger spacing (such as 0.10), in order to provide more distinguishable solutions.

### Acknowledgements

This paper is supported by the Coordination for the Improvement of Higher Education Personnel, through doctoral scholarships and project CAPES 9801-12.0 and the National Council for Scientific and Technological Development through projects CNPq 303586/2015-0 and CNPq 409318/2017-5. The authors also would like to acknowledge Prof. Ph.D. João Paulo Davim Tavares da Silva from the University of Aveiro, Portugal, who allowed and sponsored the consecution of experimental data set, the Foundation of Support Research of the State of Minas Gerais (FAPEMIG) and the anonymous reviewers for their careful reading of our paper and for their positive comments and suggestions.

### Appendix A

**Proposition.** The classic NBI formulation written as  $t$  maximization can be represented as a bi-objective problem with scaled objective functions and one equality constraint, such as:

$$\begin{array}{ll}
 \begin{array}{l}
 \text{Max}_{(x,t)} t \\
 \text{s. t. : } \bar{\mathbf{K}}\mathbf{w} + t\hat{\mathbf{n}} = \bar{\mathbf{C}}_{\text{pk}}(\mathbf{x}) \\
 \mathbf{x} \in \Omega \\
 g_j(x) \leq 0 \\
 h_j(x) = 0
 \end{array} & = \text{is equivalent to} & \begin{array}{l}
 \text{Min}_{\mathbf{x}} \bar{\mathbf{C}}_{\text{pk}}^{-1}(\mathbf{x}) \\
 \text{s. t. : } g_i(\mathbf{x}) = \bar{\mathbf{C}}_{\text{pk}}^{-1}(\mathbf{x}) - \bar{\mathbf{C}}_{\text{pk}}^2(\mathbf{x}) + 2w - 1 = 0 \\
 g_j(\mathbf{x}) \leq 0 \\
 h_{j+1}(x) = 0 \\
 \mathbf{x} \in \Omega
 \end{array}
 \end{array} \tag{A.1}$$

Proof. To prove that the aforementioned equality is true let's first prove that the maximization NBI problem is equivalent to its minimization, such as:

$$\begin{array}{ll}
 \begin{array}{l}
 \text{Max}_{(x,t)} t \\
 \text{s. t. : } \bar{\mathbf{K}}\mathbf{w} + t\hat{\mathbf{n}} = \bar{\mathbf{C}}_{\text{pk}}(\mathbf{x}) \\
 \mathbf{x} \in \Omega \\
 g_j(x) \leq 0 \\
 h_j(x) = 0
 \end{array} & = & \begin{array}{l}
 \text{Min}_{(x,t)} -t \\
 \text{s. t. : } \bar{\mathbf{K}}\mathbf{w} + t\hat{\mathbf{n}} = \bar{\mathbf{C}}_{\text{pk}}(\mathbf{x}) \\
 \mathbf{x} \in \Omega \\
 g_j(x) \leq 0 \\
 h_j(x) = 0
 \end{array}
 \end{array} \tag{A.2}$$

Let's apply the Karush-Kuhn-Tucker (KKT) optimality conditions to the NBI formulation, writing the Lagrangean of the maximization problem,  $L_1\{x, t, \lambda\}$ , and taking its partial derivatives, such that:

$$L_1\{x, t, \lambda\} = t + \lambda[\bar{\mathbf{K}}\mathbf{w} + t\hat{\mathbf{n}} - \bar{\mathbf{C}}_{\text{pk}}(\mathbf{x}^*)] \tag{A.3}$$

$$\nabla_x L_1\{x, t, \lambda\} = \frac{\partial L_1\{x, t, \lambda\}}{\partial x} = -\lambda \nabla_x \bar{\mathbf{C}}_{\text{pk}}(\mathbf{x}) = 0 \therefore \nabla_x \bar{\mathbf{C}}_{\text{pk}}(\mathbf{x}^*) = 0 \tag{A.4}$$

$$\nabla_t L_1\{x, t, \lambda\} = \frac{\partial L_1\{x, t, \lambda\}}{\partial t} = 1 + \lambda\hat{\mathbf{n}} = 0 \therefore \lambda = -\frac{1}{\hat{\mathbf{n}}} \tag{A.5}$$

$$\nabla_\lambda L_1\{x, t, \lambda\} = \frac{\partial L_1\{x, t, \lambda\}}{\partial \lambda} = \bar{\mathbf{K}}\mathbf{w} + t\hat{\mathbf{n}} - \bar{\mathbf{C}}_{\text{pk}}(\mathbf{x}^*) = 0 \therefore \bar{\mathbf{C}}_{\text{pk}}(\mathbf{x}^*) = \bar{\mathbf{K}}\mathbf{w} + t\hat{\mathbf{n}} \tag{A.6}$$

Analogously, taking the gradient of the Lagrangean for the minimization type of NBI method,  $L_2\{x, t, \lambda\}$ , leads to:

$$\begin{cases}
 \text{Min}_{(x,t)} -t \\
 \text{S. t. : } \bar{\mathbf{C}}_{\text{pk}}(\mathbf{x}) - \bar{\mathbf{K}}\mathbf{w} - t\hat{\mathbf{n}} = 0 \\
 \mathbf{x} \in \Omega, g_j(x) \leq 0, h_j(x) \leq 0
 \end{cases} \tag{A.7}$$

$$L_2\{x, t, \lambda\} = -t + \lambda[\bar{\mathbf{C}}_{\text{pk}}(\mathbf{x}^*) - \bar{\mathbf{K}}\mathbf{w} - t\hat{\mathbf{n}}] \tag{A.8}$$

$$\nabla L_2\{x, t, \lambda\} = \begin{bmatrix} \frac{\partial L_2\{x,t,\lambda\}}{\partial x} \\ \frac{\partial L_2\{x,t,\lambda\}}{\partial t} \\ \frac{\partial L_2\{x,t,\lambda\}}{\partial \lambda} \end{bmatrix} = \begin{bmatrix} \lambda \nabla_x \bar{\mathbf{C}}_{\text{pk}}(\mathbf{x}^*) \\ -1 - \lambda\hat{\mathbf{n}} \\ \bar{\mathbf{C}}_{\text{pk}}(\mathbf{x}^*) - \bar{\mathbf{K}}\mathbf{w} - t\hat{\mathbf{n}} \end{bmatrix} = \begin{bmatrix} 0 \\ 0 \\ 0 \end{bmatrix} \tag{A.9}$$

$$\nabla L_2\{x, t, \lambda\} = 0 \Rightarrow \begin{bmatrix} \nabla_x \bar{C}_{pk}(x^*) \\ \lambda \\ \bar{C}_{pk}(x^*) \end{bmatrix} = \begin{bmatrix} 0 \\ -\frac{1}{\hat{n}} \\ \bar{K}w + t\hat{n} \end{bmatrix} \tag{A.10}$$

Comparing Eqs. (A.4)-(A.6) to Eq. (A.10) it is straightforward that  $\nabla L_1\{x, t, \lambda\} = \nabla L_2\{x, t, \lambda\}$ . In Eq. (A.10), the value of  $\hat{n}$  should be chosen as a quasi-normal vector, such as:

$$\hat{n} = -\bar{K}e = \begin{bmatrix} 0 & -1 \\ -1 & 0 \end{bmatrix} \times \begin{bmatrix} 1 \\ 1 \end{bmatrix} = \begin{bmatrix} -1 \\ -1 \end{bmatrix} \tag{A.11}$$

Replacing this vector in the general formulation, the first NBI constraint will be formulated as:

$$\bar{C}_{pk}(x) - \bar{K}\beta - t(-\bar{K}e) = 0 \tag{A.12}$$

$$\bar{C}_{pk}(x) - \bar{K}w - t\hat{n} = \bar{C}_{pk}(x) - \bar{K}w - t(-\bar{K}e) = 0 \tag{A.13}$$

$$\bar{C}_{pk}(x) - \bar{K}w + t\bar{K}e = \bar{C}_{pk}(x) + \bar{K}(-w + te) \tag{A.14}$$

For bi-objective problems, the aforementioned formulation can be written as:

$$\bar{C}_{pk}(x) - \bar{K}(w - te) = \begin{bmatrix} \bar{C}_{pk}^1(x) \\ \bar{C}_{pk}^2(x) \end{bmatrix} + \begin{bmatrix} 0 & -1 \\ -1 & 0 \end{bmatrix} \times \begin{bmatrix} w_1 - t \\ w_2 - t \end{bmatrix} \tag{A.15}$$

$$\bar{C}_{pk}(x) - \bar{K}(w - te) = \begin{bmatrix} \bar{C}_{pk}^1(x) - w_2 + t \\ \bar{C}_{pk}^2(x) - w_1 + t \end{bmatrix} = \begin{bmatrix} 0 \\ 0 \end{bmatrix} \tag{A.16}$$

$$\begin{bmatrix} -t \\ -t \end{bmatrix} = \begin{bmatrix} \bar{C}_{pk}^1(x) - w_2 \\ \bar{C}_{pk}^2(x) - w_1 \end{bmatrix} \therefore \begin{bmatrix} \bar{C}_{pk}^1(x) - (1 - w_1) \\ \bar{C}_{pk}^2(x) - w_1 \end{bmatrix} \tag{A.17}$$

$$\bar{C}_{pk}(x) - \bar{K}(w - te) = \begin{bmatrix} -t \\ -t \end{bmatrix} = \begin{bmatrix} \bar{C}_{pk}^1(x) + w_1 - 1 \\ \bar{C}_{pk}^2(x) - w_1 \end{bmatrix} \tag{A.18}$$

Formulating the expression defined in terms of  $t$ , the first NBI constraint becomes:

$$\bar{C}_{pk}^1(x) + w_1 - 1 = \bar{C}_{pk}^2(x) - w_1 \text{ or } \bar{C}_{pk}^1(x) - \bar{C}_{pk}^2(x) + 2w_1 - 1 = 0 \tag{A.19}$$

Then:

$$\begin{cases} \underset{(x,t)}{\text{Min}} & -t \\ \text{S. t.} & \bar{C}_{pk}(x) - \bar{K}w - t\hat{n} = 0 \\ \mathbf{x} & \in \Omega \\ g_j(x) & \leq 0 \\ h_{j+1}(x) & = 0 \end{cases} = \begin{cases} \underset{x}{\text{Min}} & \bar{C}_{pk}(x) = w_1\bar{C}_{pk}^1(x) + (1 - w_1)\bar{C}_{pk}^2(x) \\ \text{St. :} & \bar{C}_{pk}^1(x) - \bar{C}_{pk}^2(x) + 2w_1 - 1 = 0 \\ \mathbf{x} & \in \Omega \\ g_j(x) & \leq 0 \\ h_{j+1}(x) & = 0 \end{cases} \tag{A.20}$$

We can note in Eq. (A.20) that  $\underset{x}{\text{Min}}[\bar{C}_{pk}(x)|w_1 = 1] = \underset{x}{\text{Min}}[\bar{C}_{pk}^1(x)]$ , then, we can rewrite Eq. (A.20) as:

$$\begin{cases} \underset{x}{\text{Min}} & \bar{C}_{pk}(x) = \bar{C}_{pk}^1(x) \\ \text{St. :} & \bar{C}_{pk}^1(x) - \bar{C}_{pk}^2(x) + 2w_1 - 1 = 0 \\ \mathbf{x} & \in \Omega \\ g_j(x) & \leq 0 \\ h_{j+1}(x) & = 0 \end{cases} \tag{A.21}$$

### Appendix B

**Proposition.** The probability of type II error is given by:

$$\beta_{risk} = \Phi\left(Z_{\alpha/2} - \frac{\delta\sqrt{n}}{\sigma}\right) - \Phi\left(-Z_{\alpha/2} - \frac{\delta\sqrt{n}}{\sigma}\right) \tag{B.1}$$

Proof. Let's first consider the definition of Z statistic:

$$Z_0 = \frac{\bar{X} - \mu_0}{\sigma/\sqrt{n}} = \frac{\sqrt{n}(\bar{X} - \mu_0)}{\sigma} = \frac{\sqrt{n}[(\bar{X} - \mu_0 + \delta) - \delta]}{\sigma} \tag{B.2}$$

Summing and subtracting a given value  $\delta$  from  $Z_0$ , we have:

$$Z_0 = \frac{\sqrt{n}(\bar{X} - \mu_0)}{\sigma} = \frac{\sqrt{n}[(\bar{X} - \mu_0 + \delta) - \delta]}{\sigma} \tag{B.3}$$

Then, algebraically:

$$Z_0 = \frac{\sqrt{n}[(\bar{X} - \mu_0 + \delta) - \delta]}{\sigma} = \frac{\sqrt{n}[\bar{X} - (\mu_0 + \delta) + \delta]}{\sigma} \tag{B.4}$$

$$Z_0 = \frac{\sqrt{n}[\bar{X} - (\mu_0 + \delta)]}{\sigma} + \frac{\delta\sqrt{n}}{\sigma} = \frac{\bar{X} - (\mu_0 + \delta)}{\sigma/\sqrt{n}} + \frac{\delta\sqrt{n}}{\sigma} \tag{B.5}$$

Thus, the type II error can be written as:

$$\beta_{risk} = P(-Z_{\alpha/2} \leq Z_0 \leq Z_{\alpha/2}) = P(-Z_{\alpha/2} \leq \frac{\bar{X} - (\mu_0 + \delta)}{\sigma/\sqrt{n}} + \frac{\delta\sqrt{n}}{\sigma} \leq Z_{\alpha/2}) \tag{B.6}$$

$$\beta_{risk} = P(-Z_{\alpha/2} - \frac{\delta\sqrt{n}}{\sigma} \leq \frac{\bar{X} - (\mu_0 + \delta)}{\sigma/\sqrt{n}} \leq Z_{\alpha/2} - \frac{\delta\sqrt{n}}{\sigma}) \tag{B.7}$$

$$\beta_{risk} = \Phi(Z_{\alpha/2} - \frac{\delta\sqrt{n}}{\sigma}) - \Phi(-Z_{\alpha/2} - \frac{\delta\sqrt{n}}{\sigma}) \tag{B.8}$$

### Appendix C

**Proposition.** The standard deviation of the proposed  $C_{pk}(\mathbf{x})$  is given by:

$$[SD(C_{pk}(\mathbf{x}))] = \sqrt{\frac{1}{9} + \frac{d^2}{54(N-1)\sigma^2\mathbf{x}_0(\mathbf{X}^T\mathbf{X})^{-1}\mathbf{x}_0}} \tag{C.1}$$

Where:  $d = USL - f(x)$  or  $d = f(x) - LSL$ , and  $N$  is the number of experimental data.

Proof. Let's first consider the theoretical relation of Coefficients of Variance (CV) for ratios [69]:

If  $a = b/c$ , then:

$$[CV(a)]^2 = [CV(b)]^2 + [CV(c)]^2 \tag{C.2}$$

Considering  $a = C_{pk}(\mathbf{x})$ , then:

$$b = USL - f(x), \text{ if the original response variable must be minimized.} \tag{C.3}$$

$$b = f(x) - LSL, \text{ if the original response variable must be maximized} \tag{C.4}$$

$$c = 3\sigma\sqrt{\mathbf{x}_0(\mathbf{X}^T\mathbf{X})^{-1}\mathbf{x}_0}, \text{ for both cases.} \tag{C.5}$$

Let's consider the case for  $b = USL - f(x)$ . Replacing Eqs. (C.3) and (C.5) in Eq. (C.2), we obtain:

$$[CV(C_{pk}(\mathbf{x}))]^2 = [CV(USL - f(x))]^2 + [CV(3\sigma\sqrt{\mathbf{x}_0(\mathbf{X}^T\mathbf{X})^{-1}\mathbf{x}_0})]^2 \tag{C.6}$$

We know that CV is defined as the ratio of standard deviation to the mean:

$$CV = \frac{\sigma}{\mu} \tag{C.7}$$

Therefore, each CV can be evaluated as follows:

$$\begin{aligned} [CV(USL - f(x))]^2 &= \left[\frac{SD(USL - f(x))}{E(USL - f(x))}\right]^2 \\ &= \frac{VAR(f(x))}{[E(USL - f(x))]^2} \\ &= \frac{\sigma^2\mathbf{x}_0(\mathbf{X}^T\mathbf{X})^{-1}\mathbf{x}_0}{[E(USL - f(x))]^2} \\ &= \frac{\sigma^2\mathbf{x}_0(\mathbf{X}^T\mathbf{X})^{-1}\mathbf{x}_0}{[USL - E(f(x))]^2} \\ &\approx \frac{\sigma^2\mathbf{x}_0(\mathbf{X}^T\mathbf{X})^{-1}\mathbf{x}_0}{[USL - f(x)]^2} \end{aligned} \tag{C.8}$$

$$\begin{aligned}
 [CV(3\sigma\sqrt{\mathbf{x}_0(\mathbf{X}^T\mathbf{X})^{-1}\mathbf{x}_0})]^2 &= \left[\frac{SD(3\sigma\sqrt{\mathbf{x}_0(\mathbf{X}^T\mathbf{X})^{-1}\mathbf{x}_0})}{E(3\sigma\sqrt{\mathbf{x}_0(\mathbf{X}^T\mathbf{X})^{-1}\mathbf{x}_0})}\right]^2 \\
 &= \frac{VAR(3\sigma\sqrt{\mathbf{x}_0(\mathbf{X}^T\mathbf{X})^{-1}\mathbf{x}_0})}{[E(3\sigma\sqrt{\mathbf{x}_0(\mathbf{X}^T\mathbf{X})^{-1}\mathbf{x}_0})]^2} \\
 &= \frac{VAR(3\sigma\sqrt{\mathbf{x}_0(\mathbf{X}^T\mathbf{X})^{-1}\mathbf{x}_0})}{(3\sigma\sqrt{\mathbf{x}_0(\mathbf{X}^T\mathbf{X})^{-1}\mathbf{x}_0})^2} \\
 &= \frac{(3\sigma^2\mathbf{x}_0(\mathbf{X}^T\mathbf{X})^{-1}\mathbf{x}_0)}{9\sigma^2\mathbf{x}_0(\mathbf{X}^T\mathbf{X})^{-1}\mathbf{x}_0} \\
 &= \frac{1}{6(N-1)}
 \end{aligned} \tag{C.9}$$

Replacing Eqs. (C.8) and (C.9) in Eq. (C.6), we obtain:

$$[CV(\underline{C}_{pk}(\mathbf{x}))]^2 = \frac{\sigma^2\mathbf{x}_0(\mathbf{X}^T\mathbf{X})^{-1}\mathbf{x}_0}{[USL - f(x)]^2} + \frac{1}{6(N-1)} \tag{C.10}$$

$$[CV(\underline{C}_{pk}(\mathbf{x}))] = \sqrt{\frac{\sigma^2\mathbf{x}_0(\mathbf{X}^T\mathbf{X})^{-1}\mathbf{x}_0}{[USL - f(x)]^2} + \frac{1}{6(N-1)}} \tag{C.11}$$

$$\left[\frac{SD(\underline{C}_{pk}(\mathbf{x}))}{E(\underline{C}_{pk}(\mathbf{x}))}\right] = \sqrt{\frac{\sigma^2\mathbf{x}_0(\mathbf{X}^T\mathbf{X})^{-1}\mathbf{x}_0}{[USL - f(x)]^2} + \frac{1}{6(N-1)}} \tag{C.12}$$

Multiplying Eq. (C.12) by  $E(\underline{C}_{pk}(\mathbf{x}))$ , we have:

$$[SD(\underline{C}_{pk}(\mathbf{x}))] = E(\underline{C}_{pk}(\mathbf{x}))\sqrt{\frac{\sigma^2\mathbf{x}_0(\mathbf{X}^T\mathbf{X})^{-1}\mathbf{x}_0}{[USL - f(x)]^2} + \frac{1}{6(N-1)}} \tag{C.13}$$

$$[SD(\underline{C}_{pk}(\mathbf{x}))] = \underline{C}_{pk}(\mathbf{x})\sqrt{\frac{\sigma^2\mathbf{x}_0(\mathbf{X}^T\mathbf{X})^{-1}\mathbf{x}_0}{[USL - f(x)]^2} + \frac{1}{6(N-1)}} \tag{C.14}$$

$$[SD(\underline{C}_{pk}(\mathbf{x}))] = \frac{[USL - f(x)]}{3\sigma\sqrt{\mathbf{x}_0(\mathbf{X}^T\mathbf{X})^{-1}\mathbf{x}_0}}\sqrt{\frac{\sigma^2\mathbf{x}_0(\mathbf{X}^T\mathbf{X})^{-1}\mathbf{x}_0}{[USL - f(x)]^2} + \frac{1}{6(N-1)}} \tag{C.15}$$

$$[SD(\underline{C}_{pk}(\mathbf{x}))] = \sqrt{\frac{[USL - f(x)]^2}{9\sigma^2\mathbf{x}_0(\mathbf{X}^T\mathbf{X})^{-1}\mathbf{x}_0} + \frac{[USL - f(x)]^2}{9\sigma^2\mathbf{x}_0(\mathbf{X}^T\mathbf{X})^{-1}\mathbf{x}_0} \frac{1}{6(N-1)}} \tag{C.16}$$

$$[SD(\underline{C}_{pk}(\mathbf{x}))] = \sqrt{\frac{1}{9} + \frac{[USL - f(x)]^2}{54(N-1)\sigma^2\mathbf{x}_0(\mathbf{X}^T\mathbf{X})^{-1}\mathbf{x}_0}} \tag{C.17}$$

The demonstration can also be performed for  $b = f(x) - LSL$ , giving the following expression:

$$[SD(\underline{C}_{pk}(\mathbf{x}))] = \sqrt{\frac{1}{9} + \frac{[f(x) - LSL]^2}{54(N-1)\sigma^2\mathbf{x}_0(\mathbf{X}^T\mathbf{X})^{-1}\mathbf{x}_0}} \tag{C.18}$$

Therefore, we can generalize Eqs. (C.17) and (C.18):

$$[SD(\underline{C}_{pk}(\mathbf{x}))] = \sqrt{\frac{1}{9} + \frac{d^2}{54(N-1)\sigma^2\mathbf{x}_0(\mathbf{X}^T\mathbf{X})^{-1}\mathbf{x}_0}} \tag{C.19}$$

where  $d = USL - f(x)$  or  $d = f(x) - LSL$ , and  $N$  is the number of experimental data.

**References**

[1] Chaubey SK, Jain NK. Analysis and multi-response optimization of gear quality and surface finish of meso-sized helical and bevel gears manufactured by WSEM process. *Precis Eng* 2019;55:293–309 <https://doi.org/10.1016/j.precisioneng.2018.09.019>.  
 [2] Safieddin Ardebili SM, Solmaz H, Mostafaei M. Optimization of fusel oil – gasoline blend ratio to enhance the performance and reduce emissions. *Appl Therm Eng* 2019;148:1334–45 <https://doi.org/10.1016/j.applthermaleng.2018.12.005>.  
 [3] Myers RH, Montgomery DC, Vining GG, Borror CM, Kowalski SM. Response surface methodology: a retrospective and literature survey. *J Qual Technol* 2004;36:53–77 <https://doi.org/10.1080/00224065.2004.11980252>.  
 [4] Box GEP, Draper NR. Response surfaces, mixtures, and ridge analyses. second ed. Hoboken: John Wiley & Sons; 2007.  
 [5] Park HJ, Park SH. Extension of central composite design for second-order response surface model building. *Commun Stat Theor Methods* 2010;39:1202–11 <https://doi.org/10.1080/03610920902871412>.  
 [6] Borkowski JJ. Spherical prediction variance properties of central composite and Box-Behnken designs. *Technometrics* 1995;37:399–410 <https://doi.org/10.1080/00401706.1995.10484373>.  
 [7] Box GEP, Hunter JS. Multi-factor experimental designs for exploring response surfaces. *Ann Math Stat* 1957;28:195–241 <https://doi.org/10.1214/aoms/1177707047>.

[8] Gupta K, Jain NK. Analysis and optimization of micro-geometry of miniature spur gears manufactured by wire electric discharge machining. *Precis Eng* 2014;38:728–37 <https://doi.org/10.1016/j.precisioneng.2014.03.009>.  
 [9] Huang C, Radi B, Hami A. Uncertainty analysis of deep drawing using surrogate model based probabilistic method. *Int J Adv Manuf Technol* 2016;86:3229–40 <https://doi.org/10.1007/s00170-016-8436-4>.  
 [10] Nam JS, Kim DH, Chung H, Lee SW. Optimization of environmentally benign micro-drilling process with nanofluid minimum quantity lubrication using response surface methodology and genetic algorithm. *J Clean Prod* 2015;102:428–36 <https://doi.org/10.1016/j.jclepro.2015.04.057>.  
 [11] Hebble TL, Mitchell TJ. “Repairing” response surface designs. *Technometrics* 1972;14:767–79 <https://doi.org/10.1080/00401706.1972.10488965>.  
 [12] Kumar KR, Sreebalaji VS. Modeling and analysis on the influence of reinforcement particle size during EDM of aluminum (Al/3.25Cu/8.5Si)/Fly ash composites. *J Adv Manuf Syst* 2016;15:189–207 <https://doi.org/10.1142/S0219686716500141>.  
 [13] Senthilkumar B, Kannan T. Effect of flux cored arc welding process parameters on bead geometry in super duplex stainless steel claddings. *Measurement* 2015;62:127–36 <https://doi.org/10.1016/j.measurement.2014.11.007>.  
 [14] Verma GC, Kala P, Pandey PM. Experimental investigations into internal magnetic abrasive finishing of pipes. *Int J Adv Manuf Technol* 2017;88:1657–68 <https://doi.org/10.1007/s00170-017-1657-6>.

- [org/10.1007/s00170-016-8881-0](https://doi.org/10.1007/s00170-016-8881-0).
- [15] Ajith PM, Husain TMA, Sathya P, Aravindan S. Multi-objective optimization of continuous drive friction welding process parameters using response surface methodology with intelligent optimization algorithm. *Journal of Iron and Steel Research International* 2015;22:954–60 [https://doi.org/10.1016/S1006-706X\(15\)30096-0](https://doi.org/10.1016/S1006-706X(15)30096-0).
- [16] Ariæe S, Tutunchi A, Kianvash A, Entezami AA. Modeling and optimization of mechanical behavior of bonded composite-steel single lap joints by response surface methodology. *Int J Adhesion Adhes* 2014;54:30–9 <https://doi.org/10.1016/j.ijadhadh.2014.05.002>.
- [17] Costa DMD, Paula TI, Silva PAP, Paiva AP. Normal boundary intersection method based on principal components and Taguchi's signal-to-noise ratio applied to the multiobjective optimization of 12L14 free machining steel turning process. *Int J Adv Manuf Technol* 2016;87:825–34 <https://doi.org/10.1007/s00170-016-8478-7>.
- [18] Boyacı San FG, Okur O. The effect of compression molding parameters on the electrical and physical properties of polymer composite bipolar plates. *Int J Hydrogen Energy* 2017;42:23054–69 <https://doi.org/10.1016/j.ijhydene.2017.07.175>.
- [19] Karthikeyan S, Balasubramanian V, Rajendran R. Developing empirical relationships to estimate porosity and microhardness of plasma-sprayed YSZ coatings. *Ceram Int* 2014;40:3171–83 <https://doi.org/10.1016/j.ceramint.2013.09.125>.
- [20] Safeen W, Hussain S, Wasim A, Jahanzaib M, Aziz H, Abdalla H. Predicting the tensile strength, impact toughness, and hardness of friction stir-welded AA6061-T6 using response surface methodology. *Int J Adv Manuf Technol* 2016;87:1765–81 <https://doi.org/10.1007/s00170-016-8565-9>.
- [21] Giovannitti-Jensen A, Myers RH. Graphical assessment of the prediction capability of response surface designs. *Technometrics* 1989;31:159–71 <https://doi.org/10.1080/00401706.1989.10488510>.
- [22] Myers RH, Montgomery DC. *Response Surface Methodology: process and product optimization using designed experiments*. third ed. New York: John Wiley & Sons; 2009.
- [23] Khuri AI, Cornell JA. *Response surface: design and analyses*. second ed. New York: Marcel Dekker Inc.; 1996.
- [24] Box GEP, Draper NR. A basis for the selection of a response surface design. *J Am Stat Assoc* 1959;54:622–54.
- [25] Anderson-Cook CM, Borror JM, Montgomery DC. Response surface design evaluation and comparison. *J Stat Plan Inference* 2009;139:629–41 <https://doi.org/10.1016/j.jspi.2008.04.004>.
- [26] Piepel GF. Discussion of "Response surface design evaluation and comparison" by C.M. Anderson-Cook, C.M. Borror, and D.C. Montgomery. *J Stat Plan Inference* 2009;139:653–65 <https://doi.org/10.1016/j.jspi.2008.04.008>.
- [27] Liang L, Anderson-Cook CM, Robinson TJ, Myers RH. Three-dimensional variance dispersion graphs for split-plot designs. *J Comput Graph Stat* 2006;15:757–78 <https://doi.org/10.1198/>.
- [28] Borror CM, Montgomery DC, Myers RH. Evaluation of statistical designs for experiments involving noise variables. *J Qual Technol* 2002;34:54–70 <https://doi.org/10.1080/00224065.2002.11980129>.
- [29] Montgomery DC. *Introduction to statistical quality control*. seventh ed. New York: John Wiley & Sons; 2012.
- [30] Spiring FA. A unifying approach to process capability indices. *J Qual Technol* 1997;29:49–58 <https://doi.org/10.1080/00224065.1997.11979724>.
- [31] Kotz S, Lovelace CR. *Process capability indices in theory and practice*. London: Arnold; 1998.
- [32] Rimantho D, Hanantya MW. *IOP Conf Ser Mater Sci Eng* 2017;277: 012055 <https://doi.org/10.1088/1757-899X/277/1/012055>.
- [33] Chen KS, Yu KT, Sheu SH. Process capability monitoring chart with an application in the silicon-filler manufacturing process. *Int J Prod Econ* 2006;103:565–71 <https://doi.org/10.1016/j.ijpe.2005.11.004>.
- [34] Gaudêncio JHD, Almeida FA, Sabioni RC, Turrioni JB, Paiva AP, Campos PHS. Fuzzy multivariate mean square error in equispaced pareto frontiers considering manufacturing process optimization problems. *Eng Comput* 2018 <https://doi.org/10.1007/s00366-018-0660-0>.
- [35] Das I, Dennis JE. A closer look at drawbacks of minimizing weighted sums of objectives for Pareto set generation in multicriteria optimization problems. *Struct Optim* 1997;14:63–9 <https://doi.org/10.1007/BF01197559>.
- [36] Brito TG, Paiva AP, Ferreira JR, Gomes JHF, Balestrassi PP. A normal boundary intersection approach to multiresponse robust optimization of the surface roughness in end milling process with combined arrays. *Precis Eng* 2014;38:628–38 <https://doi.org/10.1016/j.precisioneng.2014.02.013>.
- [37] Costa DMD, Brito TG, Paiva AP, Leme RC, Balestrassi PP. A normal boundary intersection with multivariate mean square error approach for dry end milling process optimization of the AISI 1045 steel. *J Clean Prod* 2016;135:1658–72 <https://doi.org/10.1016/j.jclepro.2016.01.062>.
- [38] Liu C, Gong Z, Teo KL, Feng E. Multi-objective optimization of nonlinear switched time-delay systems in fed-batch process. *Appl Math Model* 2016;40:10533–48 <https://doi.org/10.1016/j.apm.2016.07.010>.
- [39] Messac A, Ismail-Yahaya A, Mattson CA. The normalized normal constraint method for generating the Pareto frontier. *Struct Multidiscip Optim* 2003;25:86–98 <https://doi.org/10.1007/s00158-002-0276-1>.
- [40] Logist F, Houska B, Diehl M, Impe JV. Fast Pareto set generation for nonlinear optimal control problems with multiple objectives. *Struct Multidiscip Optim* 2010;42:591–603 <https://doi.org/10.1007/s00158-010-0506-x>.
- [41] Antipova E, Pozo C, Guillén-Gosálbez G, Boer D, Cabeza LF, Jiménez L. On the use of filters to facilitate the post-optimal analysis of the Pareto solutions in multi-objective optimization. *Comput Chem Eng* 2015;74:48–58 <https://doi.org/10.1016/j.compchemeng.2014.12.012>.
- [42] Medina-González S, Pozo C, Corsano G, Guillén-Gosálbez G, Espuña A. Using pareto filters to support risk management in optimization under uncertainty: application to the strategic planning of chemical supply chains. *Comput Chem Eng* 2017;98:236–55 <https://doi.org/10.1016/j.compchemeng.2016.10.008>.
- [43] Rao SS. *Engineering optimization: theory and practice*. fourth ed. Upper Saddle River: John Wiley & Sons; 2009.
- [44] Gaudêncio JHD, Almeida FA, Turrioni JB, Quinino RC, Balestrassi PP, Paiva AP. A multiobjective optimization model for machining quality in the AISI 12L14 steel turning process using fuzzy multivariate mean square error. *Precision Engineering* 2019 <https://doi.org/10.1016/j.precisioneng.2019.01.001>.
- [45] Rocha LCS, Paiva AP, Rotela Junior P, Balestrassi PP, Campos PHS, Davim JP. Robust weighting applied to optimization of AISI H13 hardened-steel turning process with ceramic wiper tool: a diversity-based approach. *Precis Eng* 2017;50:235–47 <https://doi.org/10.1016/j.precisioneng.2017.05.011>.
- [46] Garcia S, Cintra Y, Torres RCSR, Lima FG. Corporate sustainability management: a proposed multi-criteria model to support balanced decision-making. *J Clean Prod* 2016;136:181–96 <https://doi.org/10.1016/j.jclepro.2016.01.110>.
- [47] Jozic S, Bajic D, Celent L. Application of compressed cold air cooling: achieving multiple performance characteristics in end milling process. *J Clean Prod* 2015;100:325–32 <https://doi.org/10.1016/j.jclepro.2015.03.095>.
- [48] Zhang S, Li JF, Wang YW. Tool life and cutting forces in end milling Inconel 718 under dry and minimum quantity cooling lubrication cutting conditions. *J Clean Prod* 2012;32:81–7 <https://doi.org/10.1016/j.jclepro.2012.03.014>.
- [49] Ferreira R, Řehoř J, Lauro CH, Carou D, Davim JP. Analysis of the hard turning of AISI H13 steel with ceramic tools based on tool geometry: surface roughness, tool wear and their relation. *J Braz Soc Mech Sci Eng* 2016;38:2413–20 <https://doi.org/10.1007/s40430-016-0504-z>.
- [50] Galoppi GS, Filho MS, Batalha GF. Hard turning of tempered DIN 100Cr6 steel with coated and no coated CBN inserts. *J Mater Process Technol* 2006;179:146–53 <https://doi.org/10.1016/j.jmatprotec.2006.03.067>.
- [51] Amdouni H, Bouzaïene H, Montagne A, Nasri M, Iost A. Modeling and optimization of a ball-burnished aluminum alloy flat surface with a crossed strategy based on response surface methodology. *Int J Adv Manuf Technol* 2017;88:801–14 <https://doi.org/10.1007/s00170-016-8817-8>.
- [52] Hashmi KH, Zakria G, Raza MB, Khalil S. Optimization of process parameters for high speed machining of Ti-6Al-4V using response surface methodology. *Int J Adv Manuf Technol* 2016;85:1847–56 <https://doi.org/10.1007/s00170-015-8057-3>.
- [53] Grzesik W, Zak K, Kiszka P. Comparison of surface textures generated in hard turning and grinding operations. *Procedia CIRP* 2014;13:84–9 <https://doi.org/10.1016/j.procir.2014.04.015>.
- [54] Davim JP. *Machine of hard materials*. London: Springer; 2011.
- [55] Campos PHS, Davim JP, Ferreira JR, Paiva AP, Balestrassi PP. *The machinability of hard materials a review. Machinability of advanced materials*. 45 ed. London: John Wiley & Sons; 2014.
- [56] Gamarra JR, Diniz AE. Taper turning of super duplex stainless steel: tool life, tool wear and workpiece surface roughness. *J Braz Soc Mech Sci Eng* 2018;40:39 <https://doi.org/10.1007/s40430-018-0991-1>.
- [57] Rocha LCS, Paiva AP, Rotela Junior P, Balestrassi PP, Campos PHS. Robust multiple criteria decision making applied to optimization of AISI H13 hardened steel turning with PCBN wiper tool. *Int J Adv Manuf Technol* 2017;89:2251–68 <https://doi.org/10.1007/s00170-016-9250-8>.
- [58] Czitrom Veronica. One-Factor-at-a-Time versus designed experiments. *Am Statistician* 1999;53:126–31 <https://doi.org/10.1080/00031305.1999.10474445>.
- [59] Bouacha K, Yaltese MA, Mabrouki T, Rigal JF. Statistical analysis of surface roughness and cutting forces using response surface methodology in hard turning of AISI 52100 bearing steel with CBN tool. *Int J Refract Met Hard Mater* 2010;28:349–61 <https://doi.org/10.1016/j.jrhm.2009.11.011>.
- [60] Montgomery DC. *Designs and analysis of experiments*. ninth ed. USA: John Wiley & Sons; 2017.
- [61] Campos PHS. *DEA-OTS Methodology. A contribution to the optimum selection of tools in the Turning of Hardened ABNT H13 Doctoral Dissertation Brazil: Federal University of Itajuba*; 2015
- [62] Paiva AP, Paiva EJ, Ferreira JR, Balestrassi PP, Costa SC. A multivariate mean square error optimization of AISI 52100 hardened steel turning. *Int J Adv Manuf Technol* 2009;43:631–43 <https://doi.org/10.1007/s00170-008-1745-5>.
- [63] Karaoğlu S, Seçgin A. Sensitivity analysis of submerged arc welding process parameters. *J Mater Process Technol* 2008;202:500–7 <https://doi.org/10.1016/j.jmatprotec.2007.10.035>.
- [64] Rogov VA, Ghorbani S, Popikov AN, Polushin NI. Improvement of cutting tool performance during machining process by using different shim. *Archives of Civil and Mechanical Engineering* 2017;17:694–710 <https://doi.org/10.1016/j.acme.2017.01.008>.
- [65] Suyama DI, Diniz AE, Pederiva R. Tool vibration in internal turning of hardened steel using CBN tool. *Int J Adv Manuf Technol* 2017;88:2485–95 <https://doi.org/10.1007/s00170-016-8964-y>.
- [66] Del Castillo E. *Process Optimization: a statistical approach*. New York: Springer; 2007.
- [67] Jouini N, Revel P, Mazeran P, Bigerelle M. The ability of precision hard turning to increase rolling contact fatigue life. *Tribol Int* 2013;59:141–6 <https://doi.org/10.1016/j.triboint.2012.07.010>.
- [68] Revel P, Jouini N, Thoquenno G, Lefebvre F. High precision hard turning of AISI 52100 bearing steel. *Precis Eng* 2016;43:24–33 <https://doi.org/10.1016/j.precisioneng.2015.06.006>.
- [69] Bissel AF. How reliable is your capability index? *J R Stat Soc* 1990;39:331–40 <https://doi.org/10.2307/2347383>.